HHS Public Access

Author manuscript

Mol Microbiol. Author manuscript; available in PMC 2024 April 01.

Published in final edited form as:

Mol Microbiol. 2023 April ; 119(4): 439–455. doi:10.1111/mmi.15033.

Non-specific and specific DNA binding modes of bacterial histone, HU, separately regulate distinct physiological processes through different mechanisms

Subhash C. Verma[1], **Adam Harned**[2], **Kedar Narayan**[2], **Sankar Adhya**[1]

[1]Laboratory of Molecular Biology, Center for Cancer Research, National Cancer Institute, Bethesda, Maryland 20892

[2]Center for Molecular Microscopy, Frederick National Laboratory for Cancer Research, Frederick, Maryland 21701

SUMMARY

The histone-like protein HU plays a diverse role in bacterial physiology from the maintenance of chromosome structure to the regulation of gene transcription. HU binds DNA in a sequence-non-specific manner via two distinct binding modes: (i) random binding to any DNA through ionic bonds between surface-exposed lysine residues (K3, K18, and K83) and phosphate backbone (non-specific); (ii) preferential binding to contorted DNA of given structures containing a pair of kinks (structure-specific) through conserved proline residues (P63) that induce and/or stabilize the kinks. First, we show here that the P63-mediated structure-specific binding also requires the three lysine residues, which are needed for non-specific binding. Second, we demonstrate that substituting P63 to alanine in HU had no impact on non-specific binding but caused differential transcription of diverse genes previously shown to be regulated by HU, such as those associated with organonitrogen compound biosynthetic process, galactose metabolism, ribosome biogenesis, and cell adhesion. The structure-specific binding also helps create DNA supercoiling, which, in turn, may influence directly or indirectly the transcription of other genes. Our previous and current studies show that non-specific and structure-specific HU binding appear to have separate functions- nucleoid architecture and transcription regulation- which may be true in other DNA-binding proteins.

Graphical Abstract

Contact information. National Cancer Institute, Building 37, Room 5138, Bethesda, MD 20892-4255 (240) 760-7817, adhyas@mail.nih.gov.

AUTHOR CONTRIBUTIONS

SCV contributed to all aspects of the study, including experimental design; acquisition, analysis, and interpretation of the data, and writing the original draft of the manuscript. SA contributed to the supervision and editing of the manuscript. AH and KN contributed to electron microscopy to visualize fimbriae.

Conflict of Interest Statement: The authors declare no conflict of interest.

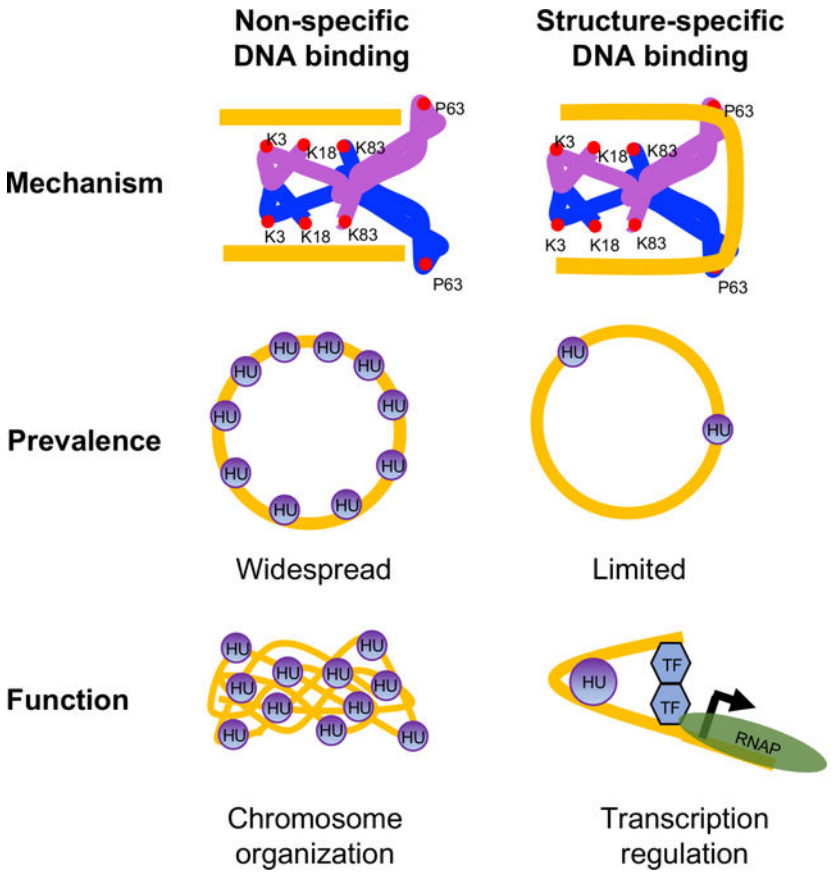

HU, the only evolutionarily conserved histone-like protein in bacteria, exhibits a non-specific or random binding mode that allows it to bind any duplex DNA without inducing bends and a DNA-structure-specific binding mode that stabilizes or indues bends in DNA. This study shows that non-specific and specific binding modes have separate functions-chromosome organization and transcription regulation, which may be true in other architectural DNA-binding proteins.

Keywords

HU; structure-specific binding; non-specific binding; transcription regulation; nucleoid architecture

INTRODUCTION

The *Escherichia coli* chromosome of 1.5-millimeter contour length is condensed and organized into a helical ellipsoid called nucleoid (Fisher et al., 2013; Verma et al., 2019). Many biochemical factors (RNA and proteins) contribute to the formation of the nucleoid (Lioy et al., 2018; Lioy et al., 2021; Verma *et al.*, 2019). Among them, the histone-like protein HU is a crucial player in maintaining a dynamic chromosome by promoting long-range DNA-DNA contacts, including the clustering of RNA-encoding loci (Lioy *et al.*, 2018; Walker et al., 2020). HU is also associated with many biological processes, including gene transcription (Aki and Adhya, 1997) and DNA metabolic reactions e.g. replication, repair,

and site-specific recombination (Chodavarapu et al., 2008; Kamashev and Rouviere-Yaniv, 2000; Montano et al., 2012). *E. coli* lacking HU exhibits a highly pleiotropic phenotype and an altered transcription profile with differential expression of about 8% of the genes (Oberto et al., 2009; Prieto et al., 2012). The HU regulon comprises highly conserved genes involved in essential biological processes, such as translation and ribosome biogenesis, and adaptive response to anaerobiosis, acid stress, and high osmolarity (Oberto *et al.*, 2009; Prieto *et al.*, 2012). Thus, HU plays a multitude of roles in bacterial physiology. Not surprisingly, HU is omnipresent in the bacterial kingdom and even essential in some bacterial species including pathogens (Bhowmick et al., 2014; Fernandez et al., 1997). HU in *E. coli* is composed of two homologous subunits α and β, encoded by *hupA* and *hupB* genes respectively, and exists in three dimeric forms: $HU\alpha_2$, $HU\beta_2$, and HUαβ. The levels of α and β subunits varies during the growth cycle, resulting in different composition of HU at different stages. $HU\alpha_2$ is predominant in the exponential phase and HUαβ in the stationary phase while $HU\beta_2$ is nearly undetectable in any growth phase (Claret and Rouviere-Yaniv, 1997).

The *E. coli* HU binds DNA in a sequence-non-specific manner with binding affinities ranging from 1 nM to up to 66,000 nM depending on DNA conformation, the form of HU, and ionic strength (Pinson et al., 1999). The extensive *in vitro* characterization of HU DNA binding using many different methodologies suggested several DNA binding modes (Hammel et al., 2016; Koh et al., 2011; Swinger et al., 2003; van Noort et al., 2004), but all of them fall into basically into two distinct types at the molecular level. We refer to them as (i) non-specific and (ii) structure-specific binding modes. The non-specific binding mode describes random binding of HU to any duplex DNA through ionic bonds between positively charged amino acid residues and phosphate backbone without inducing significant structural changes in the DNA. The structure-specific binding mode describes strong and preferential binding of HU that stabilizes or induces major DNA structural changes. The latter includes binding to contorted DNA (non-B DNA) with kinks, nicks, gaps, or cruciform structures, bent DNA within loops e.g. in the Mu transpososome and the *gal* repressosome (Bonnefoy et al., 1994; Geanacopoulos et al., 2001; Kamashev and Rouviere-Yaniv, 2000; Montano *et al.*, 2012; Pinson *et al.*, 1999; Pontiggia et al., 1993; Vitoc and Mukerji, 2011). Crystal structures of *E. coli* $HU\alpha_2$ or HUαβ bound to a 20-base pair DNA of random sequence showed that three highly conserved surface-exposed lysine residues, K3, K18, and K83, form electrostatic bonds with the DNA phosphate backbone (phosphate locks) (Fig. 1.). They are exposed on both sides of the HU dimer “body”, allowing a single HU dimer to interact simultaneously with either two different segments of the same DNA molecule or two different DNA molecules (Hammel *et al.*, 2016; Remesh et al., 2020). Crystal structures of *Anabaena* HU in a complex with a kinked DNA showed that structure-specific binding, on the other hand, involves β-strands or “arms” instead of the dimer body (Swinger *et al.*, 2003). While the positively charged surfaces of the two arms reach around the opposite faces of the DNA and wrap the minor grooves, a nearly universally conserved proline residue P63 at the tip of each arm intercalates into bases at the kink sites in the corresponding minor grooves (Swinger *et al.*, 2003) (Fig. 1). Since the kinks coincide with the intercalation of P63 residues, the intercalation must induce and/or stabilize the kinks. The binding does not involve specific amino acid-nucleobase contacts and instead solely depends on the readout of the DNA structure containing bent DNA helices, consistent with preferential

binding of HU to other forms of contorted DNA such as cruciform or nicked DNA and the binding within DNA loops e.g. in the Mu transpososome, the Hin invertasome, or the *gal* repressosome (Balandina et al., 2002; Geanacopoulos *et al.*, 2001; Kamashev et al., 1999; Montano *et al.*, 2012).

Mounting evidence suggests that HU associates with the nucleoid mostly through non-specific binding. Genomic analysis of DNA binding of the *E. coli* HU by chromatin immunoprecipitation followed by sequencing (ChIP-Seq) revealed a uniformly distributed binding profile of HU across the genome with a strong resemblance to that of mock-IP, indicating mostly weak, non-specific binding of HU to the chromosome (Prieto *et al.*, 2012). Recent studies probing the binding of HU to chromosomal DNA by single-molecule tracking demonstrated that HU exhibits fast diffusion within the nucleoid with rapid binding and unbinding to the chromosomal DNA, indicative of a weak, non-specific, and transitory binding (rapid association/dissociation kinetics) (Bettridge et al., 2020; Floc'h et al., 2019; Kamagata et al., 2021). Substituting the three lysine residues to alanine in the α subunit caused almost complete loss of HU binding to the chromosome (Bettridge *et al.*, 2020), consistent with the non-specific binding mode involving the lysine residues as shown by crystallographic studies (Hammel *et al.*, 2016; Remesh *et al.*, 2020). Substituting P63 to alanine in the α subunit had a modest effect on overall HU binding to the chromosome in the presence of the β subunit and had very little effect in the absence of the β subunit (Bettridge *et al.*, 2020), suggesting that P63-mediated structure-specific binding is not as widespread as non-specific binding and occurs at presumably a limited number of sites in the chromosome. The only demonstrated example of a structure-specific binding of HU in the *E. coli* chromosome is at the *gal* operon for regulation of the *gal* promoters. HU binds specifically between GalR binding sites (Majumdar and Adhya, 1984) and promotes the formation of a DNA loop by DNA-bound GalR-GalR interactions, blocking the transcription of the *gal* promoters located within the looped DNA (Lyubchenko et al., 1997). Furthermore, while non-specific binding is likely involved in the architectural role of HU in chromosome structure and chromosome remodeling (Hammel *et al.*, 2016; Lioy *et al.*, 2021; Remesh *et al.*, 2020), the role of structure-specific binding in HU-dependent physiological processes other than the *gal* gene regulation is unknown, leaving the role of structure-specific binding *in vivo* for further exploration. In this study, by substituting them to alanine individually or in combination, we biochemically determined the specific contribution of the lysine and P63 residues of $HU\alpha_2$ in structure-specific and non-specific DNA binding. We then examined the effect of the substitutions on three HU-dependent physiological processes, plasmid DNA supercoiling, *gal* gene expression, and global gene expression. We found that non-specific DNA binding uses only the lysine residues, corroborating the structural studies, but structure-specific binding of $HU\alpha_2$ to an artificially designed cruciform DNA *in vitro* and a potential cruciform structure at the *gal* operon *in vivo* requires both P63 and lysine residues. Furthermore, the ability of $HU\alpha_2$ to induce supercoiling in a relaxed plasmid was dependent on both P63 and lysine residues, suggesting an involvement of DNA structure-specific binding in HU-induced supercoiling. More strikingly, while $HU\alpha_2$ was sufficient for HU-mediated control of gene expression, the P63A amino acid change in $HU\alpha_2$ resulted in a gene expression profile that resembled that of an HU null strain, suggesting a major role of structure-specific binding in global gene regulation by HU. We further demonstrated the

hitherto unknown role of HU in regulating fimbriae formation via transcription control of type I fimbriae genes through structure-specific binding. Our findings together with those of recent studies (Bettridge *et al.*, 2020; Floc'h *et al.*, 2019; Kamagata *et al.*, 2021) suggest that two modes of DNA binding by HU appear to have distinct physiological roles. While the widespread non-specific binding is responsible for the dynamic organization of the chromosome, likely by enabling DNA-DNA contacts, the limited structure-specific binding is responsible for gene expression control by HU, most likely by promoting the formation of local higher-order DNA structures at or near promoters.

RESULTS

Amino acid residues of HU involved in structure-specific and non-specific DNA binding

The contributions, if any, of the lysine residues in structure-specific binding, or that of the P63 residue in non-specific binding are so far unresolved. The electron density of the β arms was either not visible in the crystal structures of HU with the random dsDNA or the β arms made no contact with the DNA (Fig. 1), implying that the P63 residue was dispensable for non-specific binding (Hammel *et al.*, 2016; Remesh *et al.*, 2020). Similarly, the contorted DNA in the crystal structure of a single HU-DNA complex was not long enough to enable contact with the lysine residues (Fig. 1.) (Swinger *et al.*, 2003). We note, however, that the contorted DNA formed a pseudo-continuous helix in the crystal packing and HU dimer contacted the phosphate backbone of the neighboring DNA (Swinger *et al.*, 2003), indicating that HU probably contacts DNA beyond the kink sites in structure-specific binding, possibly via electrostatic interactions using lysine residues and or other positively charged residues. To test whether the lysine residues contribute to structure-specific binding, or vice versa, whether the P63 residue contributes to non-specific binding, we purified $HU\alpha_2$ wild-type and $HU\alpha_2$ variants with P63A single, K3A-K83A double, or K3A-K18A-K83A triple amino acid substitutions and investigated their two modes of DNA binding. Since $HU\alpha_2$ homodimer exhibits DNA binding affinities similar to HUαβ (Pinson *et al.*, 1999) and fulfills most of the roles of HUαβ heterodimer (Wada et al., 1988), we used $HU\alpha_2$ and its variants for technical ease for this study. We used a 40-bp dsDNA of random sequence (hereafter linear DNA) to measure non-specific binding and an artificially designed cruciform DNA (Vitoc and Mukerji, 2011) to measure structure-specific binding. Binding was measured and quantified in solution by fluorescence polarization, but electrophoretic mobility shift assays (EMSA) were also carried out to monitor the formation of discrete DNA-protein complexes. Binding was measured at low salt (15 mM or 30 mM NaCl) and high salt (200 mM NaCl), as reported previously (Pinson *et al.*, 1999), to distinguish weak non-specific binding mediated by electrostatic interactions from structure-specific binding. We note that the low salt concentrations used here are below the physiological ionic strength of *E. coli,* and 200 mM is within the physiological range. Wild-type $HU\alpha_2$ exhibited binding to linear DNA at low salt but no binding at high salt (Fig. 1), consistent with the previous study (Pinson *et al.*, 1999). On the other hand, wild-type $HU\alpha_2$ showed binding to cruciform DNA at both low and high salt (Fig. 1 and S1). The cruciform DNA-HU complexes migrated as four discrete bands in EMSA under low salt conditions and as two discrete bands under high salt conditions (Fig. S2), consistent with previous findings (Bonnefoy *et al.*, 1994; Pinson *et al.*, 1999). We estimated the apparent

dissociation constants (K_d) from binding curves by nonlinear curve-fitting to a Hill equation. The apparent K_d for linear DNA at 15 mM salt was 51 nM ± 4.0. Our estimate of the apparent K_d for linear DNA is much smaller than the K_d reported previously under these buffer conditions (Pinson *et al.*, 1999). The difference could be due to the much higher sensitivity of fluorescence polarization assays in detecting weak interactions directly in solution without the need to separate free and bound DNA. Also, estimates of K_d for HU binding to a linear DNA have been reported to range from 200 nM to 2500 nM, depending on the ionic strength and DNA binding assays. HU has been reported to bind a 1000 bp linear DNA non-specifically at <100 nM concentration in atomic force microscopy experiments (van Noort *et al.*, 2004). The estimated apparent K_d for cruciform DNA at high salt was 178 nM ± 22, which is about 2-fold higher than that at low salt as reported previously (Fig. 1 and S1) (Pinson *et al.*, 1999). We next measured the binding of $HU\alpha_2$ variants to linear and cruciform DNA to determine specific contributions of the lysine and P63 residues in structure-specific and non-specific DNA binding. The $HU\alpha_2$P63A protein showed moderately reduced binding to cruciform DNA at low salt (Fig. S1) but almost a two-fold lower binding affinity at high salt compared to wild-type $HU\alpha_2$ (Fig. 2 and Fig. S1) (K_d at 200 mM salt 352 nM), validating the importance of the P63 residue in structure-specific binding to a distorted DNA as suggested by crystal structures. However, we observed no difference in the binding of wild-type $HU\alpha_2$ and $HU\alpha_2$P63A proteins to linear DNA at low salt (Fig. 2). In contrast, $HU\alpha_2$K3A-K83A and $HU\alpha_2$K3A-K18A-K83A proteins showed reduced binding not only to linear DNA, as expected, but also to cruciform DNA at both low and high salt (Fig. S1). From these results, we conclude that i) the P63 residue is dispensable for non-specific binding and ii) besides the P63 residue, the lysine residues are also critical for structure-specific binding of HU to cruciform DNA.

Involvement of structure-specific binding of HU in DNA supercoil formation

HU induces negative supercoiling in a relaxed DNA in the presence of topoisomerase I (Guo and Adhya, 2007; Tanaka et al., 1995). How HU induces negative supercoiling is not fully understood. The crystal structures of HU with a contorted (artificially kinked) DNA suggest that the P63 residue may play a critical role in the formation of negative supercoils by inducing/stabilizing flexible bends with bend angles of opposite angular orientations (Swinger *et al.*, 2003). Therefore, we tested the importance of the P63 residue, and the lysine residues, in the supercoil inducing ability of HU by incubating the wild-type and variant $HU\alpha_2$ proteins with a relaxed plasmid DNA made by introducing a nick in one of the strands. After incubation, the nicks were sealed with DNA ligase, the proteins were removed, and the resulting DNA topoisomers were resolved on gels by EMSA. Wild type $HU\alpha_2$ induced supercoils at 400 nM with saturation at 1600 nM protein concentrations (Fig. 3). The $HU\alpha_2$P63A protein was significantly impaired in the ability to form supercoils even at the saturating levels of the protein, demonstrating a critical role of the P63 residue in forming DNA supercoils. We also found the lysine residues played a significant role in the process because the $HU\alpha_2$ K3A-K83A and $HU\alpha_2$ K3A-K18A-K83A harboring double and triple lysine substitutions respectively were also impaired in promoting supercoil formation (Fig. 3). Although it is unclear whether HU binds to any specific structures in the relaxed plasmid DNA, these results show that the P63-dependent highly bent binding mode of HU

is critical for inducing supercoiling. Additionally, they confirm that this mode requires the lysine residues besides the P63 residue.

Structure-specific HU binding involved in *gal* transcription

HU binds to a specific (kinked) DNA structure in the *E. coli* chromosome at the *gal* locus as part of a higher-order DNA-multiprotein complex, called repressosome, consisting of a DNA loop, HU, and GalR, that represses transcription from the *gal* promoters (Geanacopoulos *et al.*, 2001). The HU binding site (*hbs*) in the *gal* operon contains a palindrome sequence that can potentially form a cruciform structure (Fig. S3). The fact that negative supercoiling promotes the formation of a cruciform structure in a palindrome sequence and that HU repression of the *gal* operon *in vitro* requires a negatively supercoiled DNA template suggests that the cruciform structure may determine the binding specificity of HU in the *gal* system. Therefore, to validate the importance of P63 and the lysine residues in structure-specific binding of HU in a physiologically relevant system, we examined the ability of purified wild-type and variant $HU\alpha_2$ proteins to repress *in vitro* transcription from the DNA looping-sensitive *P2* promoter in a supercoiled DNA template (Lewis et al.,1999). We observed that, compared to wild-type $HU\alpha_2$ protein, the $HU\alpha_2$P63A protein showed a significantly reduced ability to repress *gal* transcription (Fig. 4A and Fig. S4), consistent with DNA binding data. Similarly, the $HU\alpha_2$K3A-K83A and $HU\alpha_2$K3A-K18A-K83A proteins also showed reduced ability to repress the transcription (Fig. 4A and Fig. S4), confirming that lysine residues also contribute to the binding.

We also investigated the involvement of the P63 and the lysine residues in the $HU\alpha_2$-mediated *gal* repression *in vivo*. To do this, we replaced the promoter of the *lac* operon in the chromosome with the *gal* promoter segment to create a *gal-lacZ* transcription reporter fusion and carried out β-galactosidase assays in cells growing exponentially in M63 minimal media. The levels of β-galactosidase activity were low in the WT strain, which carries wild-type *hupA* and *hupB* genes and thus produces a mixture of $HU\alpha_2$ homodimer and $HU\alpha\beta$ heterodimer, in the Δ*hupB* strain, which produces only $HU\alpha_2$ homodimer, and in the Δ*hupA* strain, which produces only $HU\beta_2$ homodimer (Fig. 4B), suggesting that all three forms of HU can repress the *gal* promoter equally well. However, deleting both *hupA* and *hupB* genes caused more than a 4-fold increase in the levels of β-galactosidase activity compared to the WT strain, consistent with de-repression of the *gal* promoters due to no DNA loop formation in the absence of HU (Lewis et al., 1999). The P63A substitution in $HU\alpha_2$ also de-repressed the *gal* promoter, causing a 2.5-fold increase in the levels of β-galactosidase compared to the Δ*hupB* parent strain expressing wild-type $HU\alpha_2$ (Fig. 4B). As suggested by crystal structures of the HU-DNA complexes, the P63 residues probably facilitate a DNA loop formation by inducing/stabilizing kinks in the *gal* DNA. We reasoned that glutamic acid due to its negative charge will be even more unfavorable than alanine for the intercalation into DNA bases and thus for inducing kinks in DNA. Indeed, the P63E substitution caused even more de-repression of the *gal* promoter, resulting in a 3.5-fold increase in the levels of β-galactosidase (Fig. 4B). These results demonstrate that P63 is a critical amino acid residue in $HU\alpha_2$ for binding to DNA and to promote the formation of the DNA loop at the *gal* operon. We could not ascertain the impact of substituting lysine residues because substituting lysine residues dramatically reduced the steady-state levels

of $HU\alpha_2$ protein (Fig. S5). The K3A substitution alone reduced the steady-state levels to almost half of that without any change. The triple K3A-K18A-K83A substitution resulted in almost undetectable levels of the protein (Fig. S5). The P63A substitution, however, did not reduce the steady-state levels of the protein (Fig. S5). On the contrary, the P63A substitution caused a two-fold increase in the steady-state levels of the protein. This increase in the amount of the $HU\alpha_2$ protein caused by the P63A substitution is consistent with previously reported autorepression of the transcription of the *hupA* gene by HU, which, as this data suggests, appears to be mediated by structure-specific binding of $HU\alpha_2$ to the *hupA* promoter.

Involvement of structure-specific binding in the global gene transcription

After demonstrating the role of structure-specific binding in the *gal* gene regulation, we next examined the impact of substituting the P63 residue in $HU\alpha_2$ on global gene transcription to test whether the disruption of structure-specific binding would result in the differential expression of many other HU-regulated genes (Oberto *et al.*, 2009; Prieto *et al.*, 2012). We introduced the P63A substitution in $HU\alpha_2$ fused to mVenus to test its impact on both gene expression and the association of $HU\alpha_2$ with the nucleoid. $HU\alpha_2$-mVenus showed repression of the transcription from *gal-lacZ* reporter to the same extent as $HU\alpha_2$, and the P63A substitution in $HU\alpha_2$-mVenus showed effects like those in $HU\alpha_2$ (Fig. S6), demonstrating that the mVenus fusion does not interfere with the functionality of the $HU\alpha_2$ protein. The $HU\alpha_2$P63A-mVenus protein co-localized with the chromosomal DNA just as well as the $HU\alpha_2$-mVenus protein, with a distribution pattern resembling the shape of the chromosome (Fig. S7). This result indicates that the P63 residue does not significantly contribute to the association or the confinement of HU to the nucleoid, which is largely mediated by non-specific binding through the lysine residues (Bettridge *et al.*, 2020).

We then analyzed the transcriptome of a strain expressing either $HU\alpha_2$-mVenus (*hupA-mVenus* Δ*hupB*) or $HU\alpha_2$P63A-mVenus (*hupAP63A-mVenus* Δ*hupB*) by next-generation total RNA sequencing. In addition, we analyzed the transcriptome of a wild-type strain with functional *hupA* and *hupB* genes (WT) and an HU null strain (Δ*hupA* Δ*hupB*) to identify all HU-regulated genes. Consistent with previous reports that the absence of HU causes differential expression of many genes in *E. coli* (Oberto *et al.*, 2009; Prieto *et al.*, 2012), 438 genes showed differential expression in HU null strain compared to the WT strain (Fig. 5 and Table S1). Among those genes, 203 genes showed up-regulation and 235 genes showed down-regulation. We manually assigned the differentially expressed genes (DEGs) to biological processes based on their established functions (Table 1 and Table S2) and performed a gene ontology over-representation test of DEGs. We found the enrichment of many genes involved in the organonitrogen compound biosynthetic process (amino acid, nucleotide, and biotin synthesis), translation, ribosome biogenesis, protein folding, defense response, and cell adhesion (Table S2 and Fig. S8) as reported previously (Oberto *et al.*, 2009; Prieto *et al.*, 2012). Only the *ppiD* gene, which encodes the periplasmic chaperone PpiD, showed lower expression in the Δ*hupB* strain compared to the WT strain (Fig. 5), suggesting that (i) the *ppiD* gene is regulated by $HU\beta_2$, and (ii) $HU\alpha_2$ is sufficient for HU-mediated control of global gene expression. The same result was observed in the strain expressing $HU\alpha_2$-mVenus when compared to the WT strain, except the *hupA*

gene showed about 3-fold lower expression besides the *ppiD* gene (Fig. 5), suggesting that the mVenus fusion caused the lower expression of the *hupA* gene. The *hupA* gene was indeed detected as the only differentially expressed genes in the strain expressing $HU\alpha_2$-mVenus when compared to the strain expressing $HU\alpha_2$ without the fusion (Fig. 5), confirming that the mVenus fusion caused the lower expression of the *hupA* gene. Nonetheless, since we did not observe differential expression of any other genes despite the 3-fold lower expression of the *hupA* gene that would presumably significantly lower the amount of the $HU\alpha_2$-mVenus protein, we conclude that $HU\alpha_2$-mVenus is as good as $HU\alpha_2$ in HU-mediated control of global gene expression. However, the strain expressing $HU\alpha_2$P63A-mVenus showed differential expression of 261 genes compared to the strain expressing $HU\alpha_2$-mVenus (Fig. 5 and Table S3). Among those, 201 genes including the *gal* operon genes also showed differential expression in the HU null strain, and the differential expression was in the same direction, up or down-regulation, in both strains (Table S2). Moreover, the enrichment analysis showed an overrepresentation of genes associated with the same biological processes as those in the HU null strain, such as the organonitrogen compound biosynthetic process, ribosome biogenesis, and cellular response to hydrogen peroxide (Table 1 and Fig. S8).

The P63A substitution did not disrupt structure-specific binding completely in our DNA binding assays. Therefore, we predicted that the remaining genes may not have enough differential expression to be detected as DEGs by our criteria, but their differential expression pattern would resemble that of the HU null strain. To test this prediction, we constructed the heatmap of normalized read counts (counts per million) of 438 DEGs identified in the HU null strain. We found that the overall expression pattern of these genes in the HU null strain and the strain expressing $HU\alpha_2$P63A-mVenus was strikingly similar (Fig. S9), supporting the prediction that the complete disruption of the binding may account for even more DEGs observed in the HU null host. These results show that the structure-specific HU binding regulates many genes besides the *gal* operon. HU binds not only DNA but also RNA, with a preference for RNA containing secondary structures, such as mRNA of the *rpoS* gene, encoding the stress sigma factor of RNA polymerase (Balandina et al., 2001; Balandina *et al.*, 2002). HU binding to RNA may prevent the degradation of certain mRNA species. RNA-seq measures differential expression based on the relative RNA abundance. Therefore, it is possible that lower expression of some genes caused by the loss of structure-specific binding, or the absence of HU, is due to the degradation of mRNAs of those genes in the absence of HU binding. But it does not appear to be the case because we did not observe lower expression of any of the mRNAs and the non-coding RNAs known to associate with HU (Macvanin et al., 2012).

HU regulation of type I fimbriae

To confirm that structure-specific binding of HU controls the expression of genes other than the *gal* operon, we analyzed in detail the HU regulation of genes encoding type I fimbriae using a chromosomal *fimA-gfpmut2* transcription reporter fusion. The *fimA* gene encodes the major subunit of the type 1 fimbriae and is the first gene of the *fimAICDFGH* operon. The expression of the *fim* genes in *E. coli* is phase-variable due to the inversion of a 314 bp DNA element, called the *fimS* switch, located before the *fimA* gene (Abraham

et al., 1985). The inversion of the switch between OFF and ON orientations by FimB and FimE recombinases regulates the *fim* gene expression (Klemm, 1986). GFP intensity of most wild-type cells harboring the *fimA-gfpmut2* transcription reporter resembled that of the control cells that did not harbor *fimA-gfpmut2* (Fig. 6A). However, 7% of the cells showed fluorescence intensity higher than the control cells (Fig 6A and 6B), consistent with phase variable expression of fimbriae genes. We defined these cells as *fim*$^+$ cells. The strain expressing either HUα_2 or HUβ_2 produced about the same number of *fim*$^+$ cells as the wild-type strain (Fig. 6B). However, the HU null strain produced three-fold more *fim*$^+$ cells than the wild-type strain (Fig. 6B), suggesting that HU favors the OFF orientation of the *fimS* switch in *E. coli*. To confirm the involvement of structure-specific binding of HU, we measured the number of *fim*$^+$ cells in the strain expressing the HUα_2P63A variant protein. We observed a significant increase in the number of *fim*$^+$ cells in this strain compared to the strain expressing HUα_2 (Fig. 6B). By observing cells under scanning electron microscopy, we saw one or two long appendages protruding from wild-type cells that were most likely flagella but found many smaller appendages on the surface of cells lacking HU (Fig. 7). These appendages disappeared upon the deletion of the *fim* operon, showing that these structures were type I fimbriae (Fig. 7). We directly determined the orientation of the *fimS* switch by polymerase chain reaction (PCR) amplification of the *fimS* chromosomal region followed by the HinfI restriction digestion of the PCR products (Fig. 8A). While we detected the *fim*S switch in the ON orientation in ~11% of wild-type cells or cells expressing HUα_2 or HUβ_2, ~34% of cells lacking HU had the switch in the ON orientation (Fig. 8B), consistent with the results of the *fimA-gfpmut2* reporter. We detected the switch in the ON orientation in ~18% of cells expressing HUα_2P63A, about a 1.5-fold increase compared to cells expressing HUα_2 (Fig. 8B). We conclude from these results that structure-specific binding is, directly or indirectly, involved in maintaining the OFF position of the *fimS* switch and thereby controlling the number of cells expressing type I fimbriae genes in the bacterial population.

DISCUSSION

The role of two modes of HU binding to DNA, non-specific and structure-specific, in a multitude of physiological processes that depend on HU such as chromosome structure and gene expression is poorly understood. Here, we attempted to elucidate the molecular mechanism of the two binding modes and understand their role in HU-dependent physiological processes. We provide new insight into the mechanism of structure-specific binding and propose that the non-specific and the structure-specific HU binding have distinct functions.

Non-specific binding:

In this binding, three highly conserved lysine residues in HU electrostatically interact with DNA phosphates without inducing bends in DNA (Hammel *et al.*, 2016; Remesh *et al.*, 2020). Here, we biochemically confirm the role of the lysine residues in non-specific DNA binding of HUα_2 and show that the proline residue P63, which is required for structure-specific binding, is dispensable for non-specific binding. This is consistent with crystal structures of HU bound to a random dsDNA in which only the lysine residues made ionic

contacts with the DNA. The HU "arms" in which the P63 residues are located were either not visible or made no contact with the DNA (Fig. 1) (Hammel *et al.*, 2016; Remesh *et al.*, 2020). We note that HU may also use other binding modes for non-specific binding that do not require the lysine residues, for example, using the basic saddle (Koh *et al.*, 2011). HU appears to interact with the chromosome mostly through non-specific binding as evidenced by single-molecule tracking studies (Bettridge *et al.*, 2020; Kamagata *et al.*, 2021). It diffuses along the DNA making weak, random, and transient interactions (with rapid association/dissociation kinetics). Most of the HU in which the three lysine residues, K3, K18, and K83, were substituted to alanine lost these interactions, suggesting that HU uses the binding mode involving the lysine residues. But because the lysine residues are also needed for structure-specific binding the triple lysine substitution must destroy both non-specific and structure-specific binding of HU to the chromosome. Function-wise, the widespread non-specific binding is most likely responsible for the architectural role of HU in chromosome organization demonstrated by recent studies (Lioy *et al.*, 2018; Lioy *et al.*, 2021; Walker *et al.*, 2020). The rapid kinetics of non-specific binding can allow the newly replicated genome to rapidly reorganize as the genome progressively segregates during DNA replication (Nielsen et al., 2006).

Structure-specific binding:

Structural studies previously identified the P63 amino acid residue as a critical residue for HU binding to contorted DNA (Swinger *et al.*, 2003). We have further demonstrated here that structure-specific binding of HU to a cruciform DNA *in vitro* and to a potential cruciform structure at the *gal* operon *in vivo* requires not only the P63 residue but also the lysine residues that are needed for non-specific binding. The involvement of the lysine residues is consistent with a binding mode that resembles the DNA binding mode of integration host factor (IHF) and IHF family proteins (PDB IDs: 2NP2 and 1IHF) (Mouw and Rice, 2007; Rice et al., 1996), which are almost structurally identical to HU. In this mode, the DNA is not just bound between the β "arms", but it is also bound further along to the lysine residues on both sides of HU protein (Fig. 9). The length of the bound DNA in this mode is more than the 17-bp length of the DNA in the *Anabaena* HU-DNA complex (Fig. 1), which is supported by a 34 bp highly bent binding mode observed by isothermal titration calorimetry and fluorescence energy transfer studies (Koh et al., 2008b; Koh *et al.*, 2011). Additionally, the footprinting of chemically converted HU-nuclease revealed that HU binds to a ~40 bp long segment of the *gal* DNA (Aki and Adhya, 1997). Although HU and IHF appear to use a similar binding mode, there are striking differences between the two proteins in binding specificity and DNA bending. IHF and IHF family proteins bind to a specific DNA sequence and bend DNA by 180° (Mouw and Rice, 2007; Rice *et al.*, 1996), whereas HU binds DNA independent of the sequence and induces flexible bends (bend angles vary between 10–180°) (Koh et al., 2008a; Koh *et al.*, 2011; van Noort *et al.*, 2004). Since β-arms containing P63 residues bind and bend DNA almost in an identical manner in both HU and IHF (Swinger and Rice, 2004), the differences appear to lie in how the α-helical "body" binds with the DNA. It appears that while residues such as arginine at position 46 in the α-helical body of IHF contact specific nucleobases in the cognate sequence and sharply bend the DNA (Swinger and Rice, 2004), the lysine residues in the α-helical "body" of HU make non-specific ionic bonds with the phosphate backbone,

perhaps allowing HU to bind to contorted DNA regardless of the constituent base sequence and to induce flexible bends. Interestingly, the lysine residues K18 and K83 are conserved in both α and β subunits of HU, but they are present in either α or β subunit of IHF. Since IHF exists only as a heterodimer, this indicates that non-specific contacts may not be as important in IHF as in HU and may have been even replaced by specific amino acid-nucleobase contacts, making IHF a sequence-specific DNA binding protein despite it sharing the same structure with HU.

We recently showed that substituting P63 to alanine in $HU\alpha_2$ only slightly altered the diffusive behavior of the protein in the nucleoid. The bound fraction of the variant HU determined by modeling the distribution of diffusion coefficients of individual HU molecules using Hidden Markov model was 30%, compared to 38% of the wild-type (Bettridge *et al.*, 2020), suggesting that P63-mediated structure-specific binding is a small fraction of the global HU binding to the chromosome, occurring presumably at limited sites in the chromosome. Yet, we found that while $HU\alpha_2$ was sufficient for the HU-mediated control of gene expression, the P63A change alone in $HU\alpha_2$ resulted in an overall gene expression profile that resembled that of the HU null strain with an overlap of 201 DEGs, demonstrating that the ability of HU to induce or stabilize DNA bends is critical for the role of HU in transcription regulation. We propose that a multitude of cellular processes that HU carries out are mostly due to the regulation of gene transcription through structure-specific binding to DNA at some step of the processes, which provides the molecular basis for the highly pleiotropic phenotype of HU null cells observed in previous studies. Although identifying direct targets of the binding and elucidating the molecular mechanism involved therein need further investigation, the binding may directly regulate gene expression via the following mechanisms: (i) by promoting the formation of repressosome or enhanceosome structures, which help bring a DNA-bound repressor or an activator located at a distal site to the proximity of the RNA polymerase bound at the promoter by forming a DNA loop (e.g., *gal* operon) (Lyubchenko *et al.*, 1997). Interestingly, out of 48 operons of *E. coli* predicted to be regulated by a DNA loop, 35 operons show differential expression upon deletion of HU encoding genes either in this study or previous two studies that analyzed global gene expression control by HU (Table S4) (Cournac and Plumbridge, 2013; Oberto *et al.*, 2009; Prieto *et al.*, 2012); (ii) by facilitating site-specific recombinational flipping of invertible promoter orientation (*fim* operon) as DNA inversion frequently needs HU structure-specific binding for the formation of invertasome structure (Paull et al., 1994; Wada et al., 1989); (iii) by inducing or restraining negative supercoils of the promoter regions (Berger et al., 2016). Many promoters including the *gal* promoters are heavily dependent upon a given amount of DNA superhelicity for optimal transcription (Dorman and Dorman, 2016). Alternatively, DNA superhelicity may influence a promoter indirectly by promoting the formation of repressosome, enhanceosome, or invertasome-like structures. We note that some of the differential expression caused by the disruption of structure-specific binding could reflect secondary changes in cell physiology caused by the direct effects of the binding on gene regulation. We found that the P63A change recapitulated the previously reported anucleate phenotype of HU null strain (Fig. S10).

In summary, we propose that HU intervenes in numerous physiological events in *E. coli* by two different binding modes in distinctly different mechanisms. While non-specific

binding is widespread throughout the chromosome and dictates chromosome structure, structure-specific binding occurs at limited sites in the chromosome and regulates gene expression (Fig. 9). Other architectural DNA binding proteins such as the yeast chromatin protein Nhp6A, the factor for inversion stimulation (FIS), and IHF, and even well-studied specific DNA binding proteins such as CRP display both non-specific and specific binding to the chromosome (Kamagata *et al.*, 2021; Visweswariah and Busby, 2015). Therefore, it will not be surprising if the two kinds of binding in other proteins also have distinct biological functions.

EXPERIMENTAL PROCEDURES

Media and growth conditions.

Cells were grown in M63 minimal media supplemented with 0.1% glycerol (v/v), 10 μg ml^{-1} thiamine, and 0.5 mg ml^{-1} casamino acids. Cells were grown overnight, diluted 1000-fold, and grown to A_{600} of 0.4–0.6 for all experiments.

Strains.

All *E. coli* strains are listed in Table S5 and were derived from MG1655 (Blattner et al., 1997). Primers used in this study are listed in Table S6. Strains were constructed by Lambda Red recombineering (Yu et al., 2000) using the plasmid pSIM6 (Datta et al., 2006). To introduce amino acid substitutions in the α subunit of HU, the pBAD-ccdB-kan genetic element that was PCR amplified using homology primers hupA-kan-ccdB-u2 and hupA-kan-ccdB-l2 was inserted after the stop codon of the *hupA* open reading frame. The pBAD-ccdB-kan expresses CcdB toxin under the arabinose inducible promoter pBAD and confers kanamycin resistance. The recombinants were selected on LB agar containing 1% glucose and 30 μg ml^{-1} kanamycin and verified by PCR using the primers hupA-u1 and hupA-l1 that bind outside the *hupA* gene and by the inability of the recombinants to grow on LB agar supplemented with 0.02% arabinose. In the second step, the pBAD-ccdB-kan element was replaced with a synthetic double-stranded DNA (synthesized by Integrated DNA Technologies) encoding the *hupA* gene with mutations introducing desired amino acid substitutions in the protein. Similarly, a synthetic DNA containing the *hupA* gene genetically fused to yellow fluorescent protein mVenus via the glycine-serine-isoleucine (GSI) linker was used to construct the strain with *hupA-mVenus* fusion. The recombinants were selected on LB agar with 0.02% arabinose verified by Sanger sequencing. The plasmid pSIM6 was removed by repeatedly growing the strain at 37 °C and verifying for ampicillin sensitivity. The Δ*hupB* in the genotypes mentioned in the figures refers to the *hupB11* allele (Wada *et al.*, 1988) in which the part of the *hupB* gene between EcoRV and AatI sites is replaced with a 1.4 kb HaeII DNA fragment containing the chloramphenicol-resistance (Cm^R) gene of the pACYC184 plasmid. The *hupB11* allele was transferred using P1 phage transduction. The *gal-lacZ* reporter was constructed using Lambda Red recombineering by replacing the chromosomal region of MG1655 starting from the *lacI* up to the start codon of the *lacZ* with a DNA fragment containing ampicillin resistance gene *bla*, the *gal* promoter, and the *galE* gene. The DNA fragment was amplified from the plasmid pSA813 using the primers lacI-bla-u1 and lacZ-galE-l1. The *gal-lacZ* reporter was transferred to other strains using P1 phage transduction.

Protein purification.

HU proteins used for supercoiling assays were purified by GenScript Biotech Corporation. A 6x-histidine tag containing the Enterokinase cleavage site was placed at the N-terminus. Proteins were expressed in *E. coli* strain BL21(DE3) and purified with >95% purity using Ni-NTA affinity chromatography followed by Q-Sepharose and size-exclusion chromatography. The proteins were stored in the buffer containing 50 mM Tris HCl pH 8.0, 150 mM NaCl, and 10% Glycerol. The histidine tag was cleaved by incubating 1 ml of protein (concentration in the range of 1 to 2 mg/ml) in the storage buffer additionally containing 2 mM $CaCl_2$ with 100 units of histidine-tagged Bovine Enterokinase (GenScript Biotech Corporation) at 22°C for one hour. The tag and the enzyme were removed by incubating the reaction mix for one hour at 4°C with high-affinity Ni-NTA resin (GenScript Biotech Corporation) that was prewashed and equilibrated with the protein storage buffer. The proteins were eluted by centrifugation at 1000 × g for 1 min at 4°C and analyzed by SDS PAGE.

DNA binding assays

The 6-carboxy fluorescein (6-FAM) labeled duplex DNA substrates made by annealing the following oligonucleotides (synthesized and annealed by Integrated DNA Technologies) were used for DNA binding.

linear DNA of random sequence: CCGACTAAGTACATGTGAGAATTTTGCTGCCTTCGAACCT and /56-FAM/AGGTTCGAAGGCAGCAAAATTCTCACATGTACTTAGTCGG

Cruciform DNA: CCTAGCAAGGGGCTGCTACCTTTGGTAGCAGCCTGAGCGGTGG and /56-FAM/CCACCGCTCAACTCAACTGCTTTGCAGTTGAGTCCTTGCTAGG

The binding assays were carried out in the 100 μl reaction volume containing 10 mM Tris-HCl pH 8.0, 15 % (v/v) glycerol, 0.1 mM EDTA, 15 mM, 30 mM, or 200 mM NaCl, 1 nM DNA, and varying concentrations of the protein. The reactions were incubated in 6 mm × 50 mm glass test tubes at room temperature for 2 min and then fluorescence polarization measurements were taken in the Beacon™ 2000 instrument at 25°C. Subsequently, 20 μl reaction volume was loaded onto 6% DNA retardation gels (Invitrogen), and electrophoresis was carried out at room temperature in 0.5x Tris borate buffer, pH 8.0. The gels were imaged using Bio-Rad ChemiDoc MP Imaging System. The milipolarization (mP) units were plotted in GraphPad Prism v9. The data points were fitted using the Hill slope equation

$$Y = B_{\max} \times X^h \div \left(K_d{}^h + X^h\right)$$

wherein

$B_{\max}$

is the maximum binding in the mP units,

X

is the protein concentration,

h

is the hill slope, and

K_d is the protein concentration needed to achieve the half-maximum binding at equilibrium.

In vitro transcription assay.

In vitro transcription reactions were carried out as described earlier (Lewis, 2003). Supercoiled plasmid pSA850 (40 nM) was preincubated at 37°C for 5 min with 20 nM RNA polymerase; 200 nM GalR and/or varying concentrations of wild-type $HU\alpha_2$ or its mutant variants in a total reaction volume of 50 μl containing transcription buffer (20 mM Tris-acetate/10 mM Mg acetate/50 mM NaCl) supplemented with 1 mM DTT, 1 mM ATP, and 0.8 units recombinant ribonuclease inhibitor. Transcription reactions were initiated by adding nucleotides to a final concentration of 0.1 mM GTP and CTP, 0.01 mM UTP, and 5 μCi [α−32P] UTP (1 Ci = 37 GBq). The reactions were incubated for an additional 10 min before they were terminated by the addition of an equal volume (50 μl) of loading dye (90% formamide/10 mM EDTA/0.1% xylene cyanol/0.1% bromophenol blue). Samples were heated to 90°C for 2–3 min, chilled, then loaded on an 8% sequencing gel and electrophoresed at a constant power of 60 W in TBE (90 mM Tris/64.6 mM boric acid/2.5 mM EDTA, pH 8.3). The RNAI transcripts (106 and 108 nts) were used as an internal control to normalize the relative amount of transcript from *P2* promoter.

Supercoiling assay.

The singly nicked pCG09 plasmid was prepared by incubating CsCl purified negatively supercoiled pCG09 (60 μg) in 600 μl of 1X NEB Smart Cut buffer with the nicking endonuclease Nb.BbVCI (NEB, 8.5 units) at 37 °C for 30 min. The plasmid was purified by phenol: chloroform: isoamyl alcohol extraction, recovered by standard ethanol precipitation, and dissolved in 1X buffer containing 10 mM Tris-HCl (pH 8.0), 1 mM EDTA, and 0.05 % (v/v) IGEPAL 630 (Sigma).

$HU\alpha_2$ protein and its variants were incubated with singly nicked pCG09 plasmid for 5 min in a buffer containing 50 mM HEPES-KOH (pH 7.5), 20 mM KCl, 30 mM NaCl (from protein stocks containing 150 mM NaCl), 10 mM DTT, 5 mM MgOAc, 7.5 % glycerol, 2 mM ATP-Mg and 5 ng/μL tRNA. T4 DNA ligase was added to seal the nick. The reactions were stopped by the addition of NaCl and EDTA followed by deproteination with SDS and proteinase K for 30 min at 37°C. Topoisomers were resolved on a 0.8 % agarose gel at room temperature and 23 volts for 18 hours. Gels stained with SYBR Gold and imaged by Typhoon scanner.

β-galactosidase assay.

The β-galactosidase assay was carried out using the standard protocol. Briefly, cells were diluted in Z-buffer and permeabilized by adding 100 μl chloroform and 50 μl 0.1% sodium dodecyl sulfate. The reaction was initiated by adding 0.2 ml of 4 mg/ml o-nitrophenyl-β-D-galactoside in 0.1M phosphate buffer (pH 7.0), incubated at 28°C, and stopped after sufficient yellow color developed by adding 0.5 ml 1M Na_2CO_3. 1 ml of the reaction was transferred to a centrifuge tube, spun at maximum speed to remove debris and chloroform, and the absorbance at 420 nm was recorded for each tube. The following equation was used

to calculate units of enzyme activity: $1000 \times (A_{420}) / (A_{600} \times T \times V)$ where T is the time of reaction in minutes and V is the volume of cells used in the reaction in milliliters.

RNA sequencing.

RNA isolation and sequencing were carried out as described previously (Remesh *et al.*, 2020). For total RNA isolation, a frozen pellet of cells was resuspended and homogenized in 1 ml TRIzol reagent (Life Technologies) and incubated at room temperature for 5 min. To the resuspension, 0.2 ml chloroform was added and mixed by inverting the tube for 15 seconds. The mixture was incubated at room temperature for 10 min and then centrifuged at 20,000 × g for 10 min at 4 °C. After centrifugation, ~0.6 ml of the upper phase was transferred to a new centrifuge tube containing 0.5 ml isopropanol. The mixture was incubated at room temperature for 10 min and then centrifuged at 20,000 × g for 15 min at 4 °C. After centrifugation, the supernatant was discarded and the pellet was washed twice with 1 ml 75% ethanol in Diethyl pyrocarbonate (DEPC)-treated water by centrifugation at 13,000 × g, for 5 min at 4 °C. After the second wash, the tube was left open for 10–15 min at room temperature to dry the pellet. To the pellet, 50 μl DEPC treated water was added, and the tube was left at 37 °C for 10–15 min and then the pellet was fully resuspended using a pipette. DNA was removed using TURBO DNA-free Kit (Invitrogen). The quality of total RNA was determined by electrophoresis on the TapeStation system (Agilent). Paired-end sequencing libraries were prepared with 2.5 μg of total RNA using Illumina TruSeq Stranded Total RNA library prep workflow with Ribo-Zero. Samples were pooled and sequenced on HiSeq4000 with a read length of 150. Samples were barcode demultiplexed allowing one mismatch using Bcl2fastq v2.17. The reads were trimmed for adapters and low-quality bases using Cutadapt software. Alignment of the reads to the annotated transcriptome of *E. coli* K12 MG1655 was done using STAR. Transcript abundances were calculated by RSEM, and differential expression analysis was done using the glmTreat function of edgeR. We identified differential expression based on a false discovery rate (FDR) cut-off of 0.05 and $\log_2$ (log with base 2) fold change of 1.5. The gene ontology over-representation test was performed using the clusterProfiler package implementing enrichGO fucntion. The RNA-Seq data have been deposited to the Gene Expression Omnibus (GEO) database and can be accessed with the GEO accession number GSE175465.

Fluorescence microscopy.

1 ml bacterial culture was stained with 10 μg ml^{-1} Hoechst 33342 for 10 min and centrifuged at 1000 × g for 3 min at room temperature. All supernatant was removed except the volume in microliters equal to $A_{600} \times 200$. The resuspended cells were stained with 15 μg ml^{-1} FM464 for 10 min. Cells were then spotted onto 35 mm Poly-D-Lysine coated glass petri dish (MatTek Life Sciences) and covered by M63 glycerol 1% (w/v) agarose pad. Z-sections were collected using DeltaVision imaging system (GE Healthcare) equipped with CoolSNAP_HQ2 camera. The pixel size of each image was 0.064 μm × 0.064 μm × 0.2 μm. mVenus or GFP fluorescence was detected using a fluorescein isothiocyanate (FITC) filter (excitation: 475/28; emission: 525/48) with 100% light transmission. Hoechst 33342 was detected using a 4′,6-diamidino-2-phenylindole (DAPI) filter (excitation: 390/18; emission: 435/48) with 50% light transmission. FM464 was detected using a tetramethylrhodamine filter (excitation: 542/27; emission: 597/45) with 100% light transmission. Exposure time

for Hoechst 33342 and FM464 was 0.5 s, and for mVenus was 0.2 s. The images were deconvoluted using the recommended method in the SoftWoRx software. Image quantitation was performed in ImageJ using the middle section of the z-stack. Cell length was manually measured using FM464 fluorescence. *fim*$^+$ cells were defined as cells containing GFP fluorescence after subtracting the average fluorescence intensity of cells containing no *fimA-gfp* fusion.

Scanning electron microscopy.

An aliquot of bacterial culture growing statically was carefully pipetted and gently placed onto a Sterlitech PETE membrane filter and incubated for 2 hours without disturbance or vacuum, allowing the bacteria to settle on the substrate and maintain the structural integrity of the fine fimbriae. The samples were covered to prevent contamination and drying out. The samples were then fixed in a cocktail of 4% formaldehyde and 2% glutaraldehyde in 0.1M cacodylate buffer and subsequently post-fixed using a 1% osmium tetroxide solution. They were then dehydrated in a series of graded alcohols ranging from 35% to 100% with the final dehydration completed using a Tousimis (Rockville, MD) critical point dryer. The dried samples were then coated with a thin layer of iridium using an EMITECH K575X high-resolution sputter coater and imaged with the Zeiss 450 FE-SEM (Oberkochen, DE) at 1.50kV using the InLens SE detector.

Phase switch orientation assay.

The orientation of the *fimS* switch was determined as described previously (Stentebjerg-Olesen et al., 2000). Briefly, the chromosomal region containing the *fimS* switch was amplified by PCR using the primers fimE-u1 and fimA-l1. The PCR product was purified and 2 ug DNA was cut with *Hinfl*. The digestion fragments were separated on 2% Tris-acetate-EDTA agarose gel. The intensities of 520 bp in the ON state and 423 bp in the OFF state were quantified using the ImageJ gel analysis function.

Western Blot.

HU levels were determined by Western blotting. Cells were pelleted by centrifugation and lysed by incubating at 95°C for 10 min. Proteins were separated on 4–12% Bis-tris gels (Invitrogen) and transferred to polyvinylidene difluoride (PVDF) membrane using the iBlot 2 System (Life Science Technologies). The membrane was incubated in phosphate-buffered saline with 0.1% Tween 20 (PBST) containing mouse anti-EFTU antibody (Hycult Biotech) and either rabbit anti-HU antibody (custom made by GenScript Biotech Corporation) or rabbit anti-GFP antibody (ab290; Abcam). Subsequently, the membrane was incubated with secondary fluorescent antibodies, StarBright Blue 700 Goat Anti-Rabbit IgG (Bio-Rad) and DyLight 800 Goat Anti-Mouse IgG (Bio-Rad). After antibody incubation steps, the membrane was washed twice with PBST, and imaged using the ChemiDoc imaging system (Bio-Rad). Fluorescence intensities of EFTU and HU bands were quantified using gel analysis function of ImageJ.

Supplementary Material

Refer to Web version on PubMed Central for supplementary material.

ACKNOWLEDGMENTS

This work was supported by the Intramural Research Program of the National Institutes of Health, National Cancer Institute, Center for Cancer Research to S. A. We thank Rupesh Kumar at Memorial Sloan Kettering Cancer Center for help in supercoiling assays. We thank our laboratory members for regular discussions on the subject covered here and Dale Lewis for his additional help in *in vitro* transcription assays.

REFERENCES

Abraham JM, Freitag CS, Clements JR, and Eisenstein BI (1985). An invertible element of DNA controls phase variation of type 1 fimbriae of Escherichia coli. Proc Natl Acad Sci U S A 82, 5724–5727. 10.1073/pnas.82.17.5724. [PubMed: 2863818]

Aki T, and Adhya S (1997). Repressor induced site-specific binding of HU for transcriptional regulation. The EMBO journal 16, 3666–3674. 10.1093/emboj/16.12.3666. [PubMed: 9218807]

Balandina A, Claret L, Hengge-Aronis R, and Rouviere-Yaniv J (2001). The Escherichia coli histone-like protein HU regulates rpoS translation. Molecular microbiology 39, 1069–1079. [PubMed: 11251825]

Balandina A, Kamashev D, and Rouviere-Yaniv J (2002). The bacterial histone-like protein HU specifically recognizes similar structures in all nucleic acids. DNA, RNA, and their hybrids. The Journal of biological chemistry 277, 27622–27628. 10.1074/jbc.M201978200. [PubMed: 12006568]

Bettridge K, Verma S, Weng X, Adhya S, and Xiao J (2020). Single-molecule tracking reveals that the nucleoid-associated protein HU plays a dual role in maintaining proper nucleoid volume through differential interactions with chromosomal DNA. Molecular microbiology. 10.1111/mmi.14572.

Bhowmick T, Ghosh S, Dixit K, Ganesan V, Ramagopal UA, Dey D, Sarma SP, Ramakumar S, and Nagaraja V (2014). Targeting Mycobacterium tuberculosis nucleoid-associated protein HU with structure-based inhibitors. Nature communications 5, 4124. 10.1038/ncomms5124.

Blattner FR, Plunkett G 3rd, Bloch CA, Perna NT, Burland V, Riley M, Collado-Vides J, Glasner JD, Rode CK, Mayhew GF, et al. (1997). The complete genome sequence of Escherichia coli K-12. Science (New York, N.Y.) 277, 1453–1462. 10.1126/science.277.5331.1453. [PubMed: 9278503]

Bonnefoy E, Takahashi M, and Yaniv JR (1994). DNA-binding parameters of the HU protein of Escherichia coli to cruciform DNA. Journal of molecular biology 242, 116–129. 10.1006/jmbi.1994.1563. [PubMed: 8089835]

Chodavarapu S, Felczak MM, Yaniv JR, and Kaguni JM (2008). Escherichia coli DnaA interacts with HU in initiation at the E. coli replication origin. Molecular microbiology 67, 781–792. 10.1111/j.1365-2958.2007.06094.x. [PubMed: 18179598]

Claret L, and Rouviere-Yaniv J (1997). Variation in HU composition during growth of Escherichia coli: the heterodimer is required for long term survival. Journal of molecular biology 273, 93–104. 10.1006/jmbi.1997.1310. [PubMed: 9367749]

Cournac A, and Plumbridge J (2013). DNA looping in prokaryotes: experimental and theoretical approaches. Journal of bacteriology 195, 1109–1119. 10.1128/JB.02038-12. [PubMed: 23292776]

Datta S, Costantino N, and Court DL (2006). A set of recombineering plasmids for gram-negative bacteria. Gene 379, 109–115. 10.1016/j.gene.2006.04.018. [PubMed: 16750601]

Fernandez S, Rojo F, and Alonso JC (1997). The Bacillus subtilis chromatin-associated protein Hbsu is involved in DNA repair and recombination. Molecular microbiology 23, 1169–1179. [PubMed: 9106208]

Fisher JK, Bourniquel A, Witz G, Weiner B, Prentiss M, and Kleckner N (2013). Four-dimensional imaging of E. coli nucleoid organization and dynamics in living cells. Cell 153, 882–895. 10.1016/j.cell.2013.04.006. [PubMed: 23623305]

Floc'h K, Lacroix F, Servant P, Wong YS, Kleman JP, Bourgeois D, and Timmins J (2019). Cell morphology and nucleoid dynamics in dividing Deinococcus radiodurans. Nature communications 10, 3815. 10.1038/s41467-019-11725-5.

Geanacopoulos M, Vasmatzis G, Zhurkin VB, and Adhya S (2001). Gal repressosome contains an antiparallel DNA loop. Nat Struct Biol 8, 432–436. 10.1038/87595. [PubMed: 11323719]

Guo F, and Adhya S (2007). Spiral structure of Escherichia coli HUalphabeta provides foundation for DNA supercoiling. Proceedings of the National Academy of Sciences of the United States of America 104, 4309–4314. 10.1073/pnas.0611686104. [PubMed: 17360520]

Hammel M, Amlanjyoti D, Reyes FE, Chen JH, Parpana R, Tang HY, Larabell CA, Tainer JA, and Adhya S (2016). HU multimerization shift controls nucleoid compaction. Sci Adv 2, e1600650. 10.1126/sciadv.1600650. [PubMed: 27482541]

Kamagata K, Itoh Y, Tan C, Mano E, Wu Y, Mandali S, Takada S, and Johnson RC (2021). Testing mechanisms of DNA sliding by architectural DNA-binding proteins: dynamics of single wild-type and mutant protein molecules in vitro and in vivo. Nucleic acids research 49, 8642–8664. 10.1093/nar/gkab658. [PubMed: 34352099]

Kamashev D, Balandina A, and Rouviere-Yaniv J (1999). The binding motif recognized by HU on both nicked and cruciform DNA. The EMBO journal 18, 5434–5444. 10.1093/emboj/18.19.5434. [PubMed: 10508175]

Kamashev D, and Rouviere-Yaniv J (2000). The histone-like protein HU binds specifically to DNA recombination and repair intermediates. The EMBO journal 19, 6527–6535. 10.1093/emboj/19.23.6527. [PubMed: 11101525]

Klemm P (1986). Two regulatory fim genes, fimB and fimE, control the phase variation of type 1 fimbriae in Escherichia coli. EMBO J 5, 1389–1393. [PubMed: 2874022]

Koh J, Saecker RM, and Record MT (2008a). DNA Binding Mode Transitions of Escherichia coli HU alpha beta: Evidence for Formation of a Bent DNA - Protein Complex on Intact, Linear Duplex DNA. Journal of molecular biology 383, 324–346. 10.1016/j.jmb.2008.07.024. [PubMed: 18657548]

Koh J, Saecker RM, and Record MT Jr. (2008b). DNA binding mode transitions of Escherichia coli HU(alphabeta): evidence for formation of a bent DNA--protein complex on intact, linear duplex DNA. Journal of molecular biology 383, 324–346. 10.1016/j.jmb.2008.07.024. [PubMed: 18657548]

Koh J, Shkel I, Saecker RM, and Record MT Jr. (2011). Nonspecific DNA binding and bending by HUalphabeta: interfaces of the three binding modes characterized by salt-dependent thermodynamics. Journal of molecular biology 410, 241–267. 10.1016/j.jmb.2011.04.001. [PubMed: 21513716]

Lewis DE, Geanacopoulos M, and Adhya S (1999). Role of HU and DNA supercoiling in transcription repression: specialized nucleoprotein repression complex at gal promoters in Escherichia coli. Molecular microbiology 31, 451–461. 10.1046/j.1365-2958.1999.01186.x. [PubMed: 10027963]

Lewis DEA (2003). Identification of promoters of Esherichia coli and phage in transcription section plasmid pSA850. Method Enzymol 370, 618–645.

Lioy VS, Cournac A, Marbouty M, Duigou S, Mozziconacci J, Espeli O, Boccard F, and Koszul R (2018). Multiscale Structuring of the E. coli Chromosome by Nucleoid-Associated and Condensin Proteins. Cell 172, 771–783 e718. 10.1016/j.cell.2017.12.027. [PubMed: 29358050]

Lioy VS, Junier I, and Boccard F (2021). Multiscale Dynamic Structuring of Bacterial Chromosomes. Annu Rev Microbiol 75, 541–561. 10.1146/annurev-micro-033021-113232. [PubMed: 34343019]

Lyubchenko YL, Shlyakhtenko LS, Aki T, and Adhya S (1997). Atomic force microscopic demonstration of DNA looping by GalR and HU. Nucleic acids research 25, 873–876. [PubMed: 9016640]

Macvanin M, Edgar R, Cui F, Trostel A, Zhurkin V, and Adhya S (2012). Noncoding RNAs binding to the nucleoid protein HU in Escherichia coli. Journal of bacteriology 194, 6046–6055. 10.1128/JB.00961-12. [PubMed: 22942248]

Majumdar A, and Adhya S (1984). Demonstration of two operator elements in gal: in vitro repressor binding studies. Proceedings of the National Academy of Sciences of the United States of America 81, 6100–6104. 10.1073/pnas.81.19.6100. [PubMed: 6385008]

Montano SP, Pigli YZ, and Rice PA (2012). The mu transpososome structure sheds light on DDE recombinase evolution. Nature 491, 413–417. 10.1038/nature11602. [PubMed: 23135398]

Mouw KW, and Rice PA (2007). Shaping the Borrelia burgdorferi genome: crystal structure and binding properties of the DNA-bending protein Hbb. Molecular microbiology 63, 1319–1330. 10.1111/j.1365-2958.2007.05586.x. [PubMed: 17244195]

Nielsen HJ, Li Y, Youngren B, Hansen FG, and Austin S (2006). Progressive segregation of the Escherichia coli chromosome. Molecular microbiology 61, 383–393. 10.1111/j.1365-2958.2006.05245.x. [PubMed: 16771843]

Oberto J, Nabti S, Jooste V, Mignot H, and Rouviere-Yaniv J (2009). The HU regulon is composed of genes responding to anaerobiosis, acid stress, high osmolarity and SOS induction. PloS one 4, e4367. 10.1371/journal.pone.0004367. [PubMed: 19194530]

Paull TT, Haykinson MJ, and Johnson RC (1994). HU and functional analogs in eukaryotes promote Hin invertasome assembly. Biochimie 76, 992–1004. 10.1016/0300-9084(94)90024-8. [PubMed: 7748943]

Pinson V, Takahashi M, and Rouviere-Yaniv J (1999). Differential binding of the Escherichia coli HU, homodimeric forms and heterodimeric form to linear, gapped and cruciform DNA. Journal of molecular biology 287, 485–497. 10.1006/jmbi.1999.2631. [PubMed: 10092454]

Pontiggia A, Negri A, Beltrame M, and Bianchi ME (1993). Protein HU binds specifically to kinked DNA. Molecular microbiology 7, 343–350. [PubMed: 8459763]

Prieto AI, Kahramanoglou C, Ali RM, Fraser GM, Seshasayee AS, and Luscombe NM (2012). Genomic analysis of DNA binding and gene regulation by homologous nucleoid-associated proteins IHF and HU in Escherichia coli K12. Nucleic acids research 40, 3524–3537. 10.1093/nar/gkr1236. [PubMed: 22180530]

Remesh SG, Verma SC, Chen JH, Ekman AA, Larabell CA, Adhya S, and Hammel M (2020). Nucleoid remodeling during environmental adaptation is regulated by HU-dependent DNA bundling. Nature communications 11, 2905. 10.1038/s41467-020-16724-5.

Rice PA, Yang S, Mizuuchi K, and Nash HA (1996). Crystal structure of an IHF-DNA complex: a protein-induced DNA U-turn. Cell 87, 1295–1306. [PubMed: 8980235]

Stentebjerg-Olesen B, Chakraborty T, and Klemm P (2000). FimE-catalyzed off-to-on inversion of the type 1 fimbrial phase switch and insertion sequence recruitment in an Escherichia coli K-12 fimB strain. FEMS microbiology letters 182, 319–325. 10.1111/j.1574-6968.2000.tb08915.x. [PubMed: 10620686]

Swinger KK, Lemberg KM, Zhang Y, and Rice PA (2003). Flexible DNA bending in HU-DNA cocrystal structures. The EMBO journal 22, 3749–3760. 10.1093/emboj/cdg351. [PubMed: 12853489]

Swinger KK, and Rice PA (2004). IHF and HU: flexible architects of bent DNA. Curr Opin Struct Biol 14, 28–35. 10.1016/j.sbi.2003.12.003. [PubMed: 15102446]

Tanaka H, Yasuzawa K, Kohno K, Goshima N, Kano Y, Saiki T, and Imamoto F (1995). Role of HU proteins in forming and constraining supercoils of chromosomal DNA in Escherichia coli. Molecular & general genetics : MGG 248, 518–526. 10.1007/BF02423446. [PubMed: 7476850]

van Noort J, Verbrugge S, Goosen N, Dekker C, and Dame RT (2004). Dual architectural roles of HU: formation of flexible hinges and rigid filaments. Proceedings of the National Academy of Sciences of the United States of America 101, 6969–6974. 10.1073/pnas.0308230101. [PubMed: 15118104]

Verma SC, Qian Z, and Adhya SL (2019). Architecture of the Escherichia coli nucleoid. PLoS genetics 15, e1008456. 10.1371/journal.pgen.1008456. [PubMed: 31830036]

Visweswariah SS, and Busby SJ (2015). Evolution of bacterial transcription factors: how proteins take on new tasks, but do not always stop doing the old ones. Trends in microbiology 23, 463–467. 10.1016/j.tim.2015.04.009. [PubMed: 26003748]

Vitoc CI, and Mukerji I (2011). HU binding to a DNA four-way junction probed by Forster resonance energy transfer. Biochemistry 50, 1432–1441. 10.1021/bi1007589. [PubMed: 21230005]

Wada M, Kano Y, Ogawa T, Okazaki T, and Imamoto F (1988). Construction and characterization of the deletion mutant of hupA and hupB genes in Escherichia coli. Journal of molecular biology 204, 581–591. [PubMed: 3066907]

Wada M, Kutsukake K, Komano T, Imamoto F, and Kano Y (1989). Participation of the hup gene product in site-specific DNA inversion in Escherichia coli. Gene 76, 345–352. 10.1016/0378-1119(89)90174-1. [PubMed: 2666260]

Walker DM, Freddolino PL, and Harshey RM (2020). A Well-Mixed E. coli Genome: Widespread Contacts Revealed by Tracking Mu Transposition. Cell 180, 703–716 e718. 10.1016/j.cell.2020.01.031. [PubMed: 32059782]

Yu D, Ellis HM, Lee EC, Jenkins NA, Copeland NG, and Court DL (2000). An efficient recombination system for chromosome engineering in Escherichia coli. Proceedings of the National Academy of Sciences of the United States of America 97, 5978–5983. 10.1073/pnas.100127597. [PubMed: 10811905]

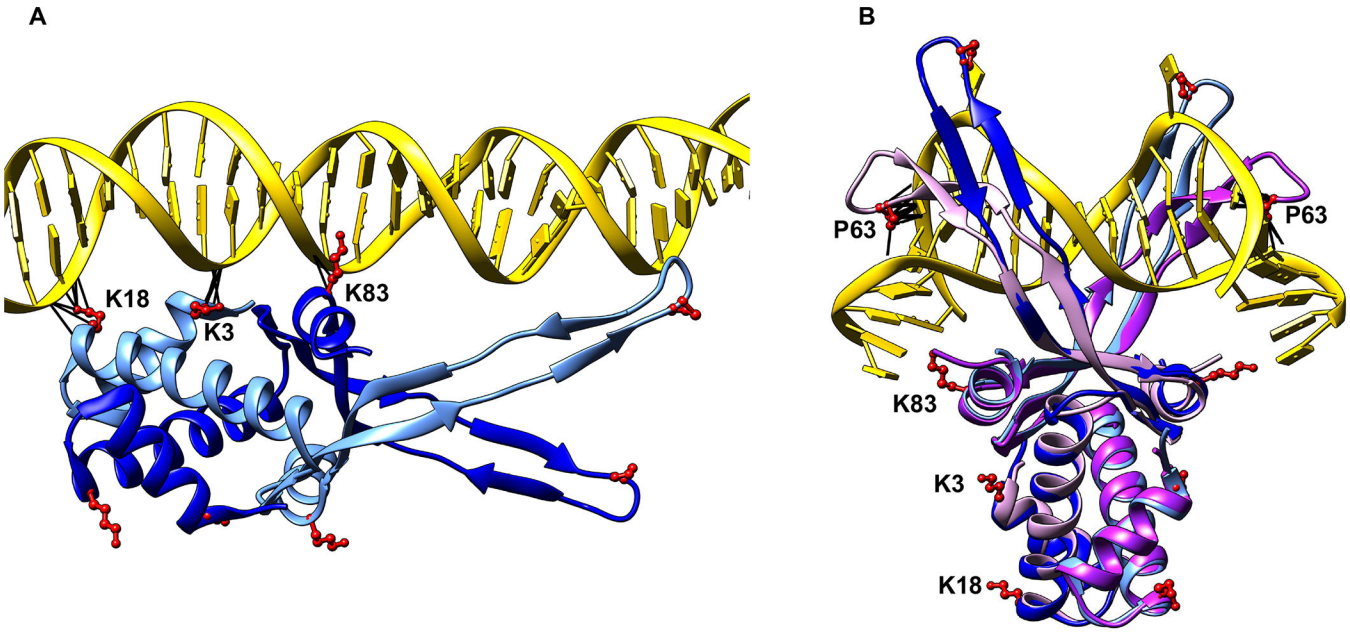

Fig. 1.

Crystal structures of HU-DNA complexes.

(A) Crystal structure of *E. coli* HUα_2 (α subunits in blue and cornflower blue) in a complex with linear DNA (PDB 6O8Q).

(B) Crystal structure of *Anabaena* HU (two subunits in plum and purple) in a complex with a distorted DNA (PDB 1P51), with *E. coli* HUα_2 (shown in A) superimposed on it. The lysine residues, K3, K18, and K83, and the proline residue P63 of both HU subunits are shown in red. Any contacts between these residues and DNA are shown as black lines.

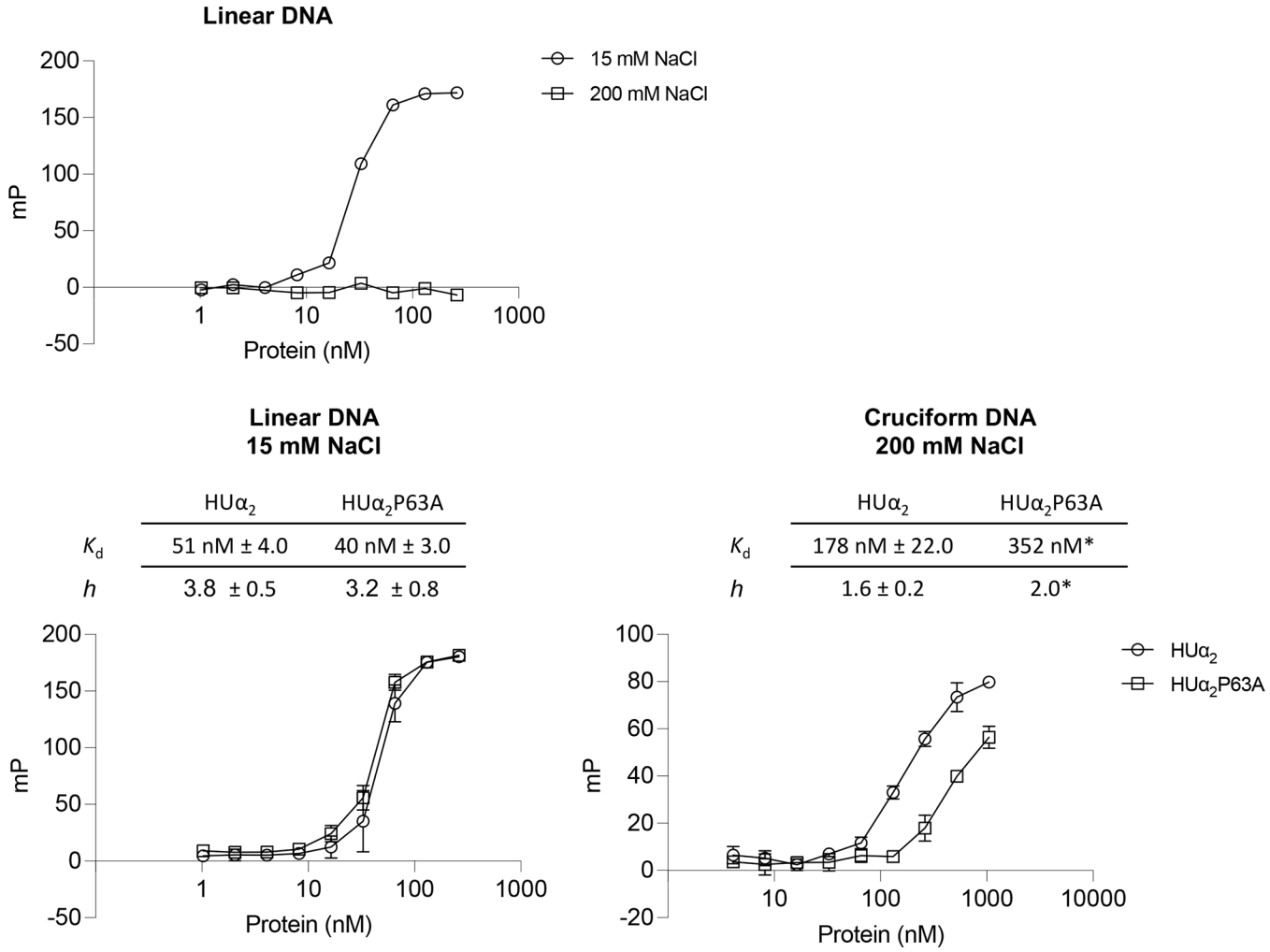

Fig. 2.

Effect of substituting lysine and P63 residues of HUα_2 on DNA binding.

Binding of purified wild-type HUα_2 or its variants harboring indicated amino acid substitutions to a 6-carboxy fluorescein labeled linear DNA or cruciform DNA. Each data point on Y-axis represents a change in milipolarization (mP) units at indicated protein concentrations in fluorescence polarizations assays. K_d (nM) estimated by fitting binding curves to a Hill equation are given in the table. ND = not determined.

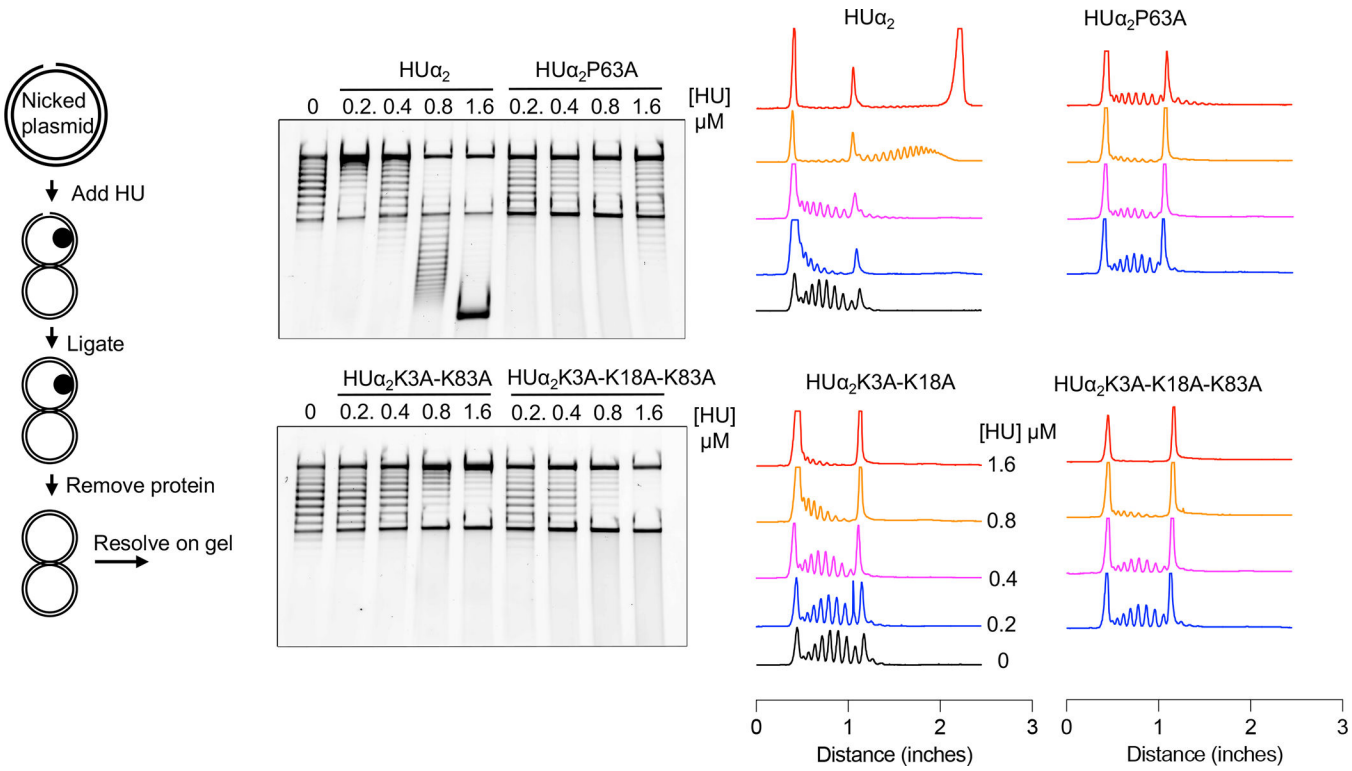

Fig. 3.

Effect of substituting lysine and P63 residues of $HU\alpha_2$ on supercoiling inducing ability. The left panel outlines the assay carried out to determine the ability of $HU\alpha_2$ to induce negative supercoils in a nicked plasmid DNA. The middle panel shows the electrophoresis of the DNA products from the assay in the presence of the indicated concentrations of wild-type $HU\alpha_2$ protein or its variants. The right panel shows densitometric lane traces of the gel shown in the middle panel.

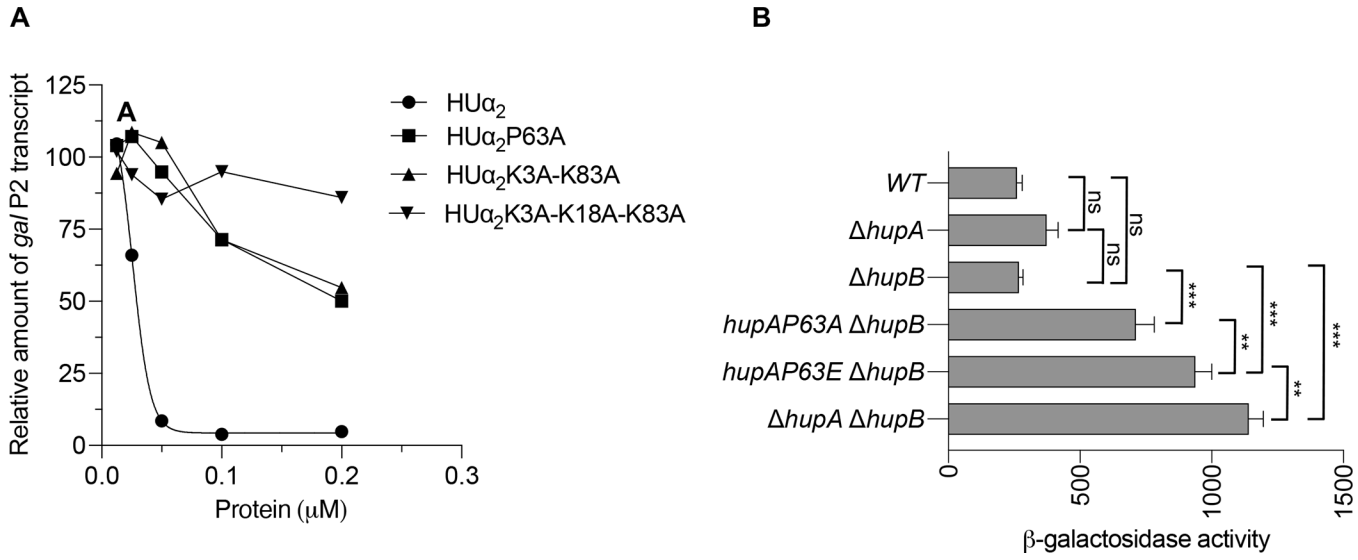

Fig. 4.

Effect of substituting lysine and P63 residues of HUα_2 on *gal* transcription

(A) Amount of *galP2* transcript originating from the *galP2* promoter of pSA850 plasmid in the presence of 200 nM GalR and the indicated concentrations of HUα_2 protein or its variants. The amount of *galP2* transcript was normalized with that of *RNAI* and *RNAII* transcripts originating from the same plasmid. Each data point represents the *galP2/(RNAI + RNAII)* transcript ratio relative to that in the presence of GalR alone which was set to 100. The gel image used to quantify transcript amount is shown in Fig. S3).

(B) Levels of β-galactosidase activity of the chromosomal *galE-lacZ* transcriptional reporter in the *E. coli* strains of indicated genotypes: Graphical and error bars represent averages and standard deviation of triplicate biological replicates, respectively. Experiment was performed twice, with similar results. Statistically significant differences were determined by 1-way ANOVA with Tukey's multiple comparisons test. *ns* not significant; ** adjusted p-value 0.001; *** adjusted p-value <0.001.

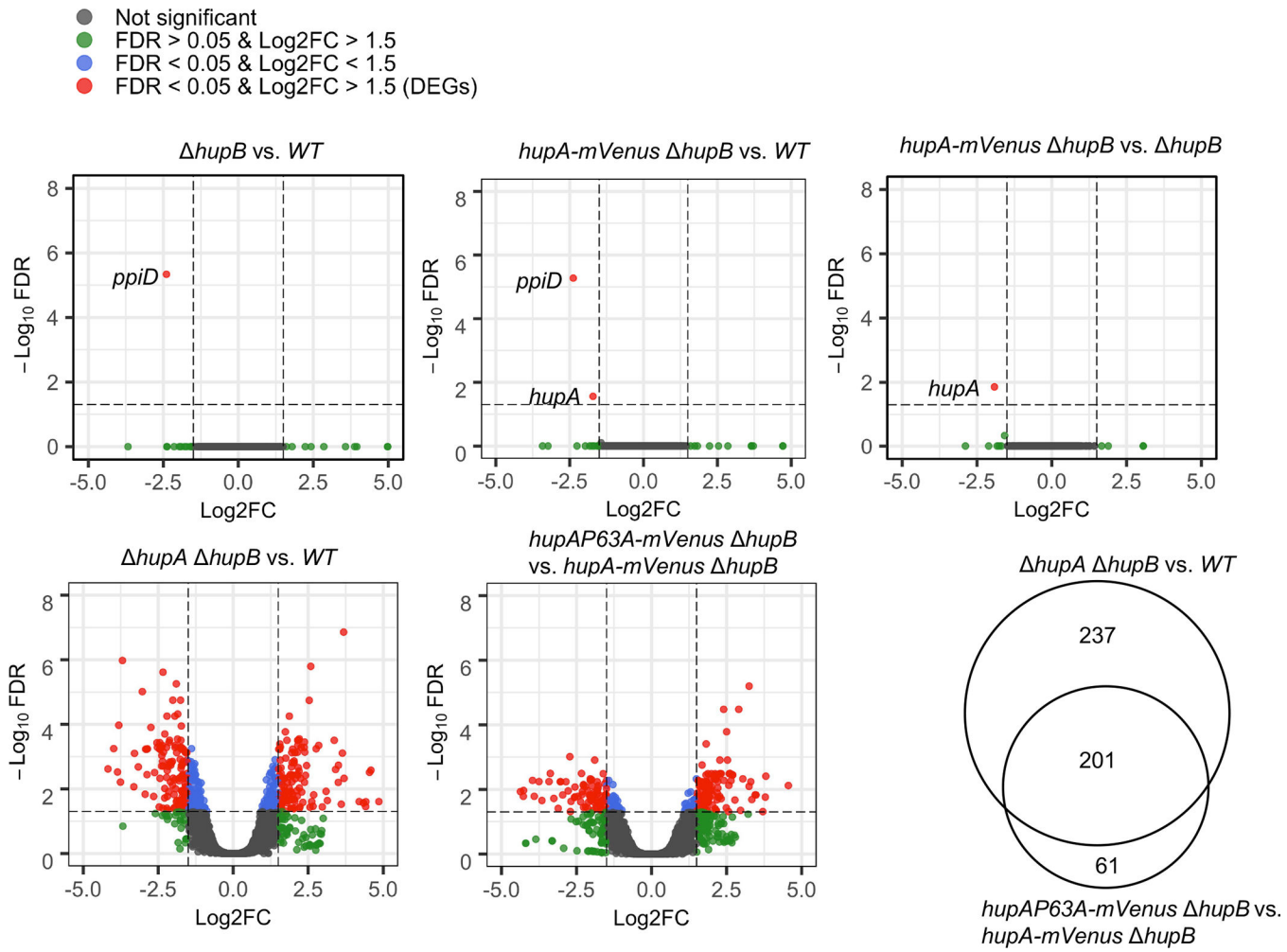

Fig. 5.

Effect of substituting the P63 residue of HUα_2 on global gene expression.

Volcano plots showing differential expression of genes between *E. coli* strains of the indicated genotypes. X-axis represents log2 of the fold-change (Log2FC) in RNA levels and y-axis represents the −log10 of false discovery rate (FDR) of each gene. Vertical dotted lines are positioned at a log2 fold-change of 0.5 or −0.5 and horizontal dotted lines are positioned at the −log10 of 0.05 FDR. Genes in red are identified as differentially expressed genes (DEGs), determined using glmTreat function at FDR<0.05 and log2 fold-change >0.5 (plus or minus). Venn diagram shows DEGs common between two the comparison groups.

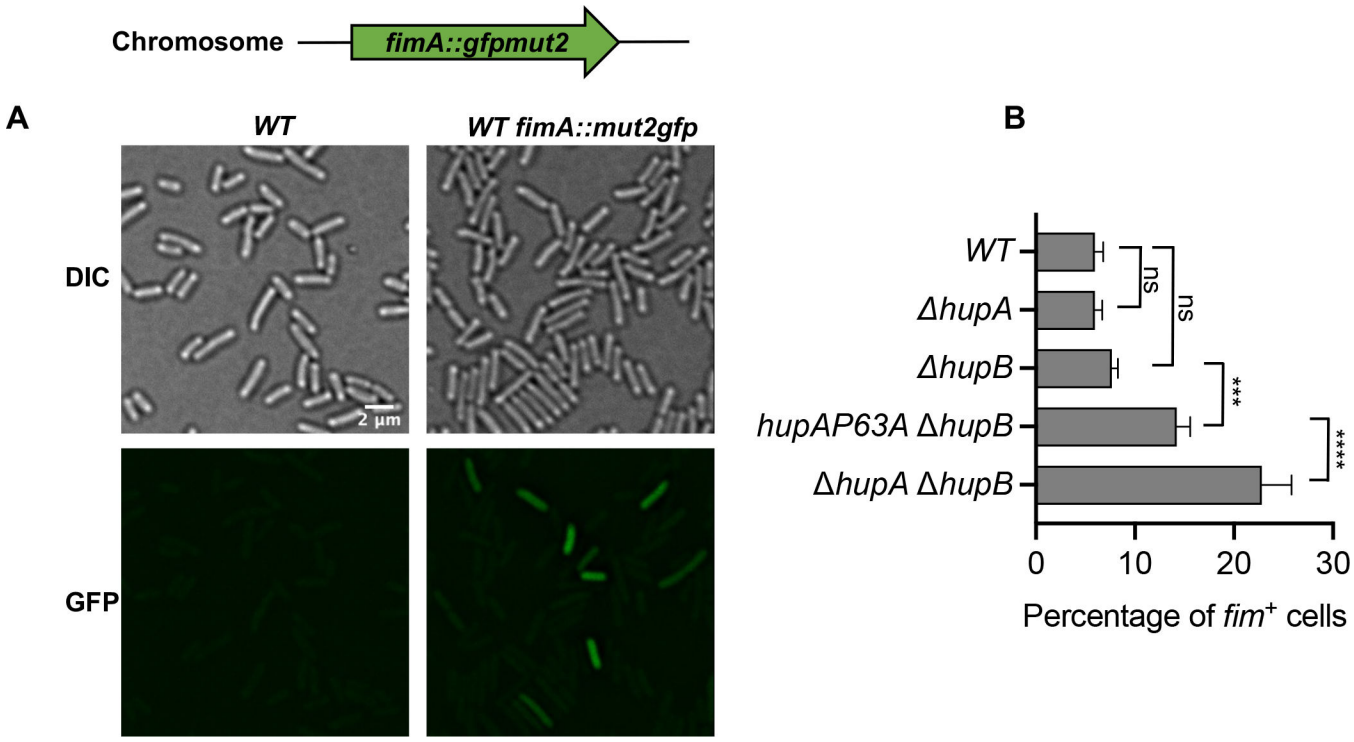

Fig. 6.

Role of HU in transcription regulation of type 1 fimbriae genes

(A) Representative fluorescence and differential interference contrast images of WT cells, or WT cells harboring *fimA::gfpmut2* transcriptional reporter.

(B) Percentage of cells expressing GFP fluorescence above background in *E. coli* strains harboring the indicated deletion mutations in *hupA* and *hupB* genes and mutations in the *hupA* gene to introduce P63A amino acid substitution in the HUα subunit. Graphical and error bars represent averages and standard deviation of at least four fluorescence images each containing more than 200 cells. Experiment was performed twice, with similar results. Statistically significant differences as determined by 1-way ANOVA with Dunnett's multiple comparisons test. *ns* not significant; *** adjusted p-value 0.0001; **** adjusted p-value <0.0001.

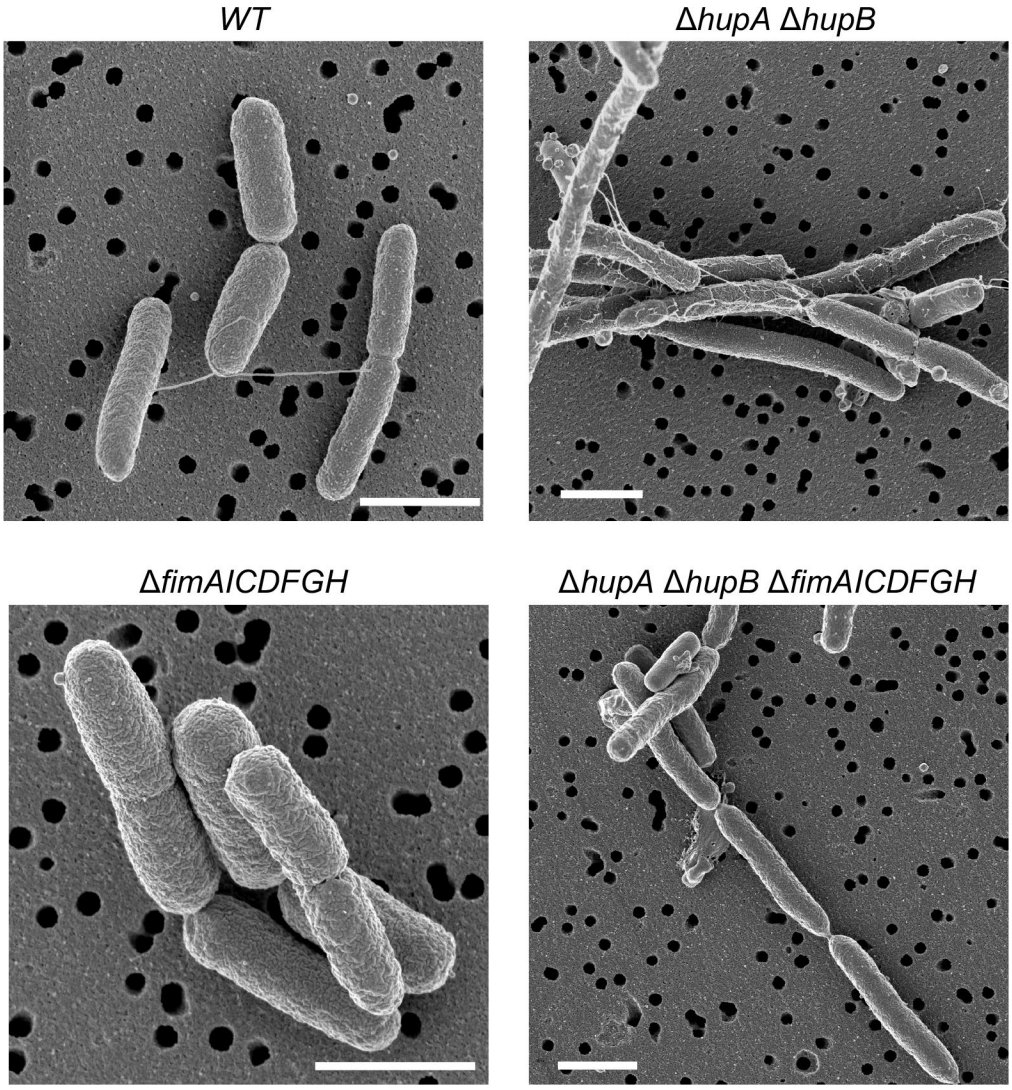

Fig. 7.

Role of HU in the formation of type I fimbriae on the surface of *E. coli* cells

Scanning electron micrographs of representative cells of *E. coli* strains harboring the indicated deletion mutations in *hupA*, *hupB*, and type I fimbriae genes. Scale bar 1 μm.

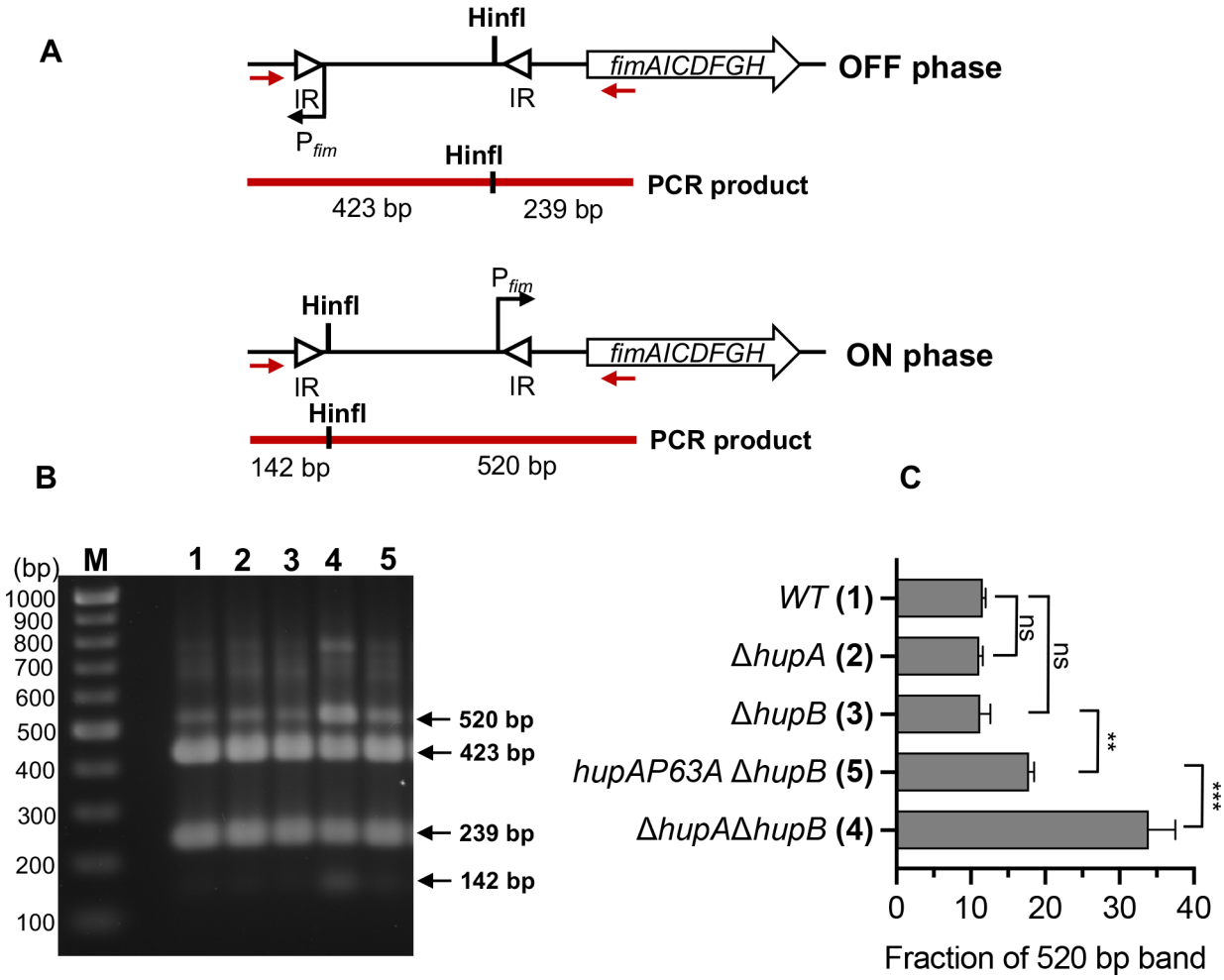

Fig. 8.

Role of HU in regulating the orientation of the *fimS* switch

(A) The position of HinfI restriction site when *fimS* switch is in ON or OFF phase. Red arrows represent the binding sites of the primers fimE-u1 and fimA-l1 used for polymerase chain reaction of *fimS* region. Solid red lines represent the PCR products and sizes of HinfI restriction fragments in ON or OFF phase. *IR* inverted repeats

(B) Agarose geel after electrophoresis of HinfI digestion reactions of the PCR products of chromosomal DNA of *E. coli* strains harboring the indicated deletion mutations in *hupA* and *hupB* genes and mutations in the *hupA* gene to introduce P63A amino acid substitution in the HUα subunit. Numbers correspond to genotypes in panel B. *M* DNA marker.

(C) Percentage amount of 520 bp fragment from total amount of 520 bp and 423 bp fragments. Graphical and error bars represent averages and standard deviation of three biological replicates respectively. Experiment was performed twice, with similar results. Statistically significant differences as determined by 1-way ANOVA with Dunnett's multiple comparisons test. *ns* not significant; ** adjusted p-value 0.003; *** adjusted p-value <0.001.

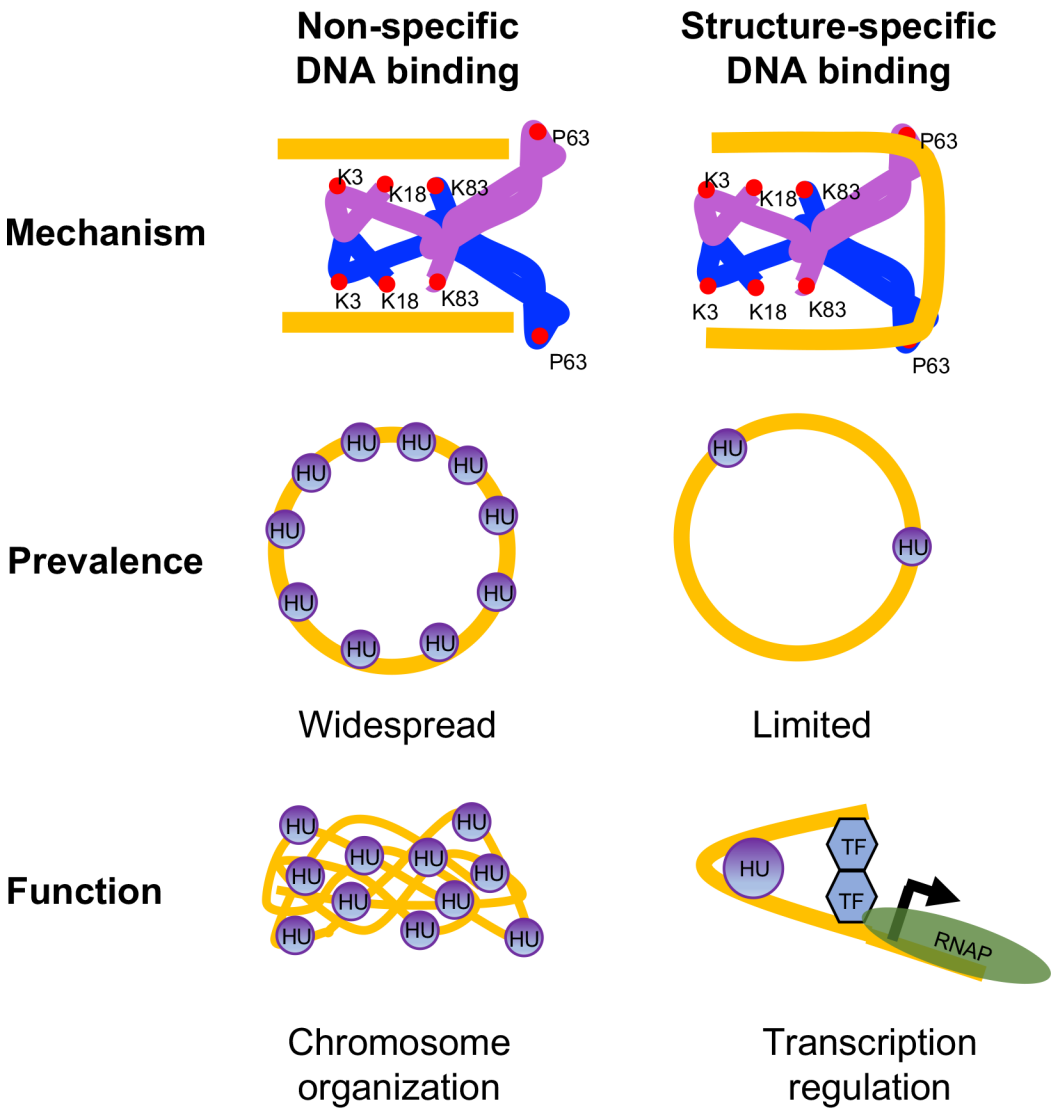

Figure 9.

A model for mechanism, prevalence, and function of non-specific and structure-specific DNA binding modes of HU in *E. coli*

Two subunits of HU are depicted as blue and purple with DNA binding amino acid residues shown as red circles. DNA is depicted in gold. The bound DNA is in the straight conformation in non-specific mode and sharpy bent in structure-specific mode. While non-specific binding mode is widespread in the chromosome and primarily involved in chromosome organization, structure-specific binding mode is limited and involved in transcription regulation. *TF* Transcription factor; *RNAP* RNA polymerase.

Table 1.

Number of genes associated with various biological processes that were differentially expressed in a E. coli strain lacking HU (relative to WT strain harboring hupA and hupB genes) or a E. coli strain producing HUα2P63A (relative to a strain producing HUα2) or both.

Biological process	***ΔhupA ΔhupB* vs. *WT***	***hupAmP63A ΔhupB* vs. *hupAm ΔhupB***	**Common**	**Total**	**Unique**
Others	111	58	45	169	124
Amino acid metabolism	42	32	28	74	46
Transport	32	11	9	43	34
Transcription/Cell signaling	31	8	6	39	33
Translation	29	28	18	57	39
Carbohydrate metabolism	28	14	10	42	32
Stress response	25	17	13	42	29
Adhesion	24	12	9	36	27
DNA metabolism	18	13	9	31	22
Nucleotide biosynthesis	16	12	9	28	19
Protein homeostasis	14	9	7	23	16
Prophage	11	7	4	18	14
Nitrate assimilation	8	2	1	10	9
ATP synthesis	7	8	7	15	8
Putrescine metabolism	7	7	7	14	7
Cell cycle	7	4	4	11	7
Biotin synthesis	6	6	6	12	6
Pseudogenes	6	3	2	9	7
Methylglyoxal catabolism	4	2	2	6	4
Fatty acid oxidation	4	2	2	6	4
Defense	4	0	0	4	4
TCA cycle	2	5	2	7	5
ncRNAs	2	1	1	3	2
	438	261	201	699	498